Phytophthora sojae effector PsAvh113 associates with the soybean transcription factor GmDPB to inhibit catalase-mediated immunity

Xiaoguo Zhu[†], Liang Guo[†], Ruiqing Zhu[†], Xiaoyi Zhou[†], Jianing Zhang, Die Li, Shidan He and Yongli Qiao* [ID]

Shanghai Key Laboratory of Plant Molecular Sciences, College of Life Sciences, Shanghai Normal University, Shanghai, China

Summary

Phytophthora species are the most destructive plant pathogens worldwide and the main threat to agricultural and natural ecosystems; however, their pathogenic mechanism remains largely unknown. Here, we show that Avh113 effector is required for the virulence of *Phytophthora sojae* and is important for development of *Phytophthora* root and stem rot (PRSR) in soybean (*Glycine max*). Ectopic expression of *PsAvh113* enhanced viral and *Phytophthora* infection in *Nicotiana benthamiana*. PsAvh113 directly associated with the soybean transcription factor GmDPB, inducing its degradation by the 26S proteasome. The internal repeat 2 (IR2) motif of PsAvh113 was important for its virulence and interaction with GmDPB, while silencing and overexpression of *GmDPB* in soybean hairy roots altered the resistance to *P. sojae*. Upon binding to GmDPB, PsAvh113 decreased the transcription of the downstream gene *GmCAT1*, which acts as a positive regulator of plant immunity. Furthermore, we revealed that PsAvh113 suppressed the *GmCAT1*-induced cell death by associating with GmDPB, thereby enhancing plant susceptibility to *Phytophthora*. Together, our findings reveal a vital role of PsAvh113 in inducing PRSR in soybean and offer a novel insight into the interplay between defence and counter-defence during the *P. sojae* infection of soybean.

Introduction

Microbial pathogens and their plant hosts are involved in a perpetual arms race, which is well demonstrated by the classical zig-zag model (Jones and Dangl, 2006). A fierce battle of attack, counter-attack and counter-counter-attack arises in the cytoplasmic space, which frequently governs the outcome of pathogen effector–plant interactions (Jones and Dangl, 2006; Wang *et al.*, 2019). *Phytophthora*, a filamentous eukaryotic pathogen, is responsible for many devastating plant diseases (Kamoun *et al.*, 2015). *Phytophthora* root and stem rot (PRSR) caused by *Phytophthora sojae* is one of the most devastating diseases of soybean (*Glycine max*), resulting in annual losses of $1–2 billion globally (Tyler *et al.*, 2006). Despite extensive studies, the mechanism of its hemibiotrophic pathogenesis is still inadequately understood. Accumulating evidence demonstrates that *P. sojae* secretes an arsenal of host cytoplasmic effectors, some of which interfere with plant innate immunity by modifying host target functions and disrupting the immune signalling network (Ai *et al.*, 2021; Hou *et al.*, 2019; Jing *et al.*, 2016; Kong *et al.*, 2017; Lin *et al.*, 2021; Lu *et al.*, 2023; Qiao *et al.*, 2013; Song *et al.*, 2015; Wang and Wang, 2018). However, the host targets and their molecular mechanisms regulated by the majority of *P. sojae* effectors remain unexplored.

DRFT1-polypeptide1 (DP1; also known as Dimerization Partner 1) belongs to a family of transcription factors that heterodimerize with E2 PROMOTER BINDING FACTOR (E2F) to bind to target DNA (Girling *et al.*, 1993). E2F, a nuclear factor in HeLa cells infected with adenovirus, is able to stimulate the early expression of the E2 virus gene, named E2F, which is responsible for gene transcription (Kovesdi *et al.*, 1987). Numerous studies have shown that DP proteins can heterodimerize with E2F to form a complex, which exhibits greater DNA-binding ability and enhances the transcription of E2F target genes by binding to the joint E2 recognition site (Helin *et al.*, 1993). The E2F/DP family of transcription factors includes typical E2Fs and atypical E2Fs (DP/ E2F-like [DEL]) as well as their related DP proteins, and plays a pivotal role in controlling the activity of cyclin-dependent kinase and the progression of cell cycle in plants and animals (Kent and Leone, 2019; Lammens *et al.*, 2009).

To date, a number of E2F family members have been identified in the animal kingdom; for example, seven E2F and two DP proteins in mammals, two E2F proteins in *Drosophila*, and one DP protein in *Caenorhabditis elegans* (Dimova and Dyson, 2005). E2F family members have also been identified in multiple plant species, including *Arabidopsis*, *Nicotiana benthamiana*, carrot and rice (Kosugi and Ohashi, 2002a). Among these plant species, *Arabidopsis* is the most well-characterized for E2F/DP proteins. Studies show that the *Arabidopsis* genome encodes three typical E2Fs (AtE2FA, AtE2FB and AtE2FC), three atypical E2Fs (AtDEL1, AtDEL2 and AtDEL3) and two DPs (AtDPA and AtDPB) (Mariconti *et al.*, 2002). For instance, AtE2FA and AtE2FB activate the expression of genes involved in the initiation and progression of the S-phase, whereas AtE2FC and AtDEL act as repressors and induce the G2 or G2/M cell cycle arrest, which potentially negatively regulates some E2F target genes involved in the G1/S-phase (Vlieghe *et al.*, 2005). However, several studies show that the E2F/DP family proteins are also involved in multiple biological processes, such as mitosis, response to DNA damage, DNA repair and cell differentiation, apoptosis and plant development

(DeGregori and Johnson, 2006). The *Arabidopsis e2fabc* triple mutant is highly susceptible to the bacterial pathogen *Pseudomonas syringae* pv. *maculicola* (Psm) strain ES4326, and does not express some of the immune response-related genes (Wang et al., 2014). *AtDEL1* participates in the immune response by regulating the expression of the *EDS5* gene, which encodes a salicylic acid (SA) transporter (Chandran et al., 2014). However, the above-mentioned studies focused on the mechanism of E2F proteins in plants and animals, and little is known about the role of DP proteins in plants.

The catalase (CAT) family consists of highly conserved enzymes that convert hydrogen peroxide (H_2O_2) into water and oxygen, and plays a critical role in the response to abiotic and biotic stresses (Petrov and Van Breusegem, 2012). Phylogenetic analysis suggests that most animals contain a single *CAT* gene, whereas angiosperms such as *N. benthamiana*, *Arabidopsis*, maize, pumpkin and rice contain three *CAT* genes (Mhamdi et al., 2010). In *Arabidopsis*, *AtCAT1* is an essential gene that responds to numerous abiotic stresses by scavenging H_2O_2. Moreover, *AtCAT2* and *AtCAT3* are involved in eliminating H_2O_2 in both light and dark conditions, leading to the homeostasis of reactive oxygen species (ROS) (Mhamdi et al., 2010). The mutation of *AtCAT2* results in enhanced resistance to bacterial pathogens, mainly because the reduced CAT activity increases H_2O_2 accumulation. Recent studies show that the accumulated SA binds to AtCAT2 to inhibit its enzymatic activity upon exposure to biotrophic pathogens (Yuan et al., 2017). Although CAT enzymes play an important role in the association with several viral effectors through distinct mechanisms (Inaba et al., 2011; Jiao et al., 2021; Mathioudakis et al., 2013; Roshan et al., 2018; Yang et al., 2020), two CRN effectors of *P. sojae* ectopically regulate programmed cell death (PCD) by disrupting CAT activity and perturbing H_2O_2 homeostasis in *N. benthamiana* (Zhang et al., 2015). Nevertheless, how *P. sojae* modulates soybean CATs to overcome host defence remains largely unexplored.

Here, we report the identification of a virulence effector of *P. sojae*, PsAvh113, using the potato virus X (PVX)-based virus-induced virulence effector (VIVE) assay, and its role in facilitating *P. sojae* infection. We show that PsAvh113 is important for *Phytophthora* infection in both *N. benthamiana* and soybean. PsAvh113 associates with the soybean transcription factor GmDPB and causes its degradation by the 26S proteasome. Furthermore, GmDPB binds directly to the promoter of *GmCAT1* and induces its expression. PsAvh113 suppressed the GmCAT1-induced cell death by associating with GmDPB. Taken together, these results indicate that PsAvh113 inhibits the expression of *GmCAT1* by associating with transcription factor GmDPB, thus enhancing the susceptibility to *P. sojae* in soybean.

Results

PsAvh113 contributes to *Phytophthora* infection in plants

To identify the key virulence effectors of *P. sojae*, we performed the VIVE rapid functional screening assay in *N. benthamiana* (Shi et al., 2020). Compared with the mock treatment, *N. benthamiana* plants infected with PVX carrying *PsAvh113* displayed strong viral symptoms and high-level viral RNA accumulation in leaves, whereas those inoculated with the empty vector displayed mild viral symptoms and lower viral RNA

abundance (Figures 1a,b and S1a). These results suggest that *PsAvh113* encodes a potential virulence effector that promotes viral infection. PsAvh113 is predicted to a typical *P. sojae* RxLR effector, and its amino acid sequence was highly conserved among various strains of *P. sojae* (Figure S1b). The expression of *PsAvh113* was significantly induced at an early stage of infection, reaching a peak at 12 h post-inoculation, which was approximately 50-fold higher than its expression at mycelia (Figure S1c).

To confirm the contribution of PsAvh113 to virulence in the host plant, the *PsAvh113* gene was transiently expressed in HC6 soybean hairy roots (Figure S1d), which were then inoculated with the RFP-labelled wild-type (WT) *P. sojae* strain P6497 (P6497-RFP). Compared with hairy roots expressing the empty vector (EV) control, those expressing *PsAvh113* produced more oospores (Figure 1c,d) and accumulated greater *P. sojae* biomass (Figure 1e). To further investigate the importance of *PsAvh113* in plant infection, we knocked out *PsAvh113* in the WT *P. sojae* strain P6497 using the CRISPR/Cas9 system. Protoplasts of *P. sojae* were co-transformed with the two unique sgRNAs (Figure S1e) and the hSpCas9 expression plasmid. Subsequently, many transformants were generated and identified by genomic DNA (gDNA)-based PCR, and three homozygous *PsAvh113* knockout mutants (C364, C404 and C540) were inoculated in soybean hypocotyls (Figure S1f). Compared with the WT strain, the three *PsAvh113* knockout mutants showed no difference in growth (Figure S1g) but had a significantly reduced ability to cause disease (Figure 1f). Furthermore, all *PsAvh113* knockout mutants of *P. sojae* caused smaller lesions on soybean seedlings than in the WT strain (Figure 1g). Consistently, *P. sojae* biomass was markedly lower in soybean seedlings infected with *PsAvh113* knockout mutants than in seedlings infected with the WT strain (Figure 1h).

The ability of *PsAvh113* to promote disease development prompted us to examine whether its expression in plants can facilitate infection. We generated two independent *Arabidopsis* transgenic lines expressing *PsAvh113* and identified by Western blotting, which exhibited dwarfed and moderately retarded development and slightly delayed flowering compared with WT plants (Figure S2a–d). Upon inoculation with *P. parasitica*, both transgenic lines showed significantly more susceptibility, higher pathogen biomass and larger lesions than WT plants (Figure S2e–g). Together, these experiments indicate that *PsAvh113* is required for full virulence of pathogen.

Internal repeat 2 (IR2) motif is required for the virulence activity of PsAvh113

Domain and motif searches using the Simple Modular Architecture Research Tool (SMART) database identified two IRs (IR1 and IR2) in the C-terminal region of PsAvh113, which differed by only one amino acid (Figure 2a). To determine the virulence role of IR motifs in PsAvh113, we generated five PsAvh113 mutant proteins, including PsAvh113$^{\triangle IR1}$ (IR1 region was substituted with alanine residues), PsAvh113$^{\triangle IR2}$ (IR2 region was substituted with alanine residues) and three residue substitution mutants of PsAvh113 which substituted Ser108 with Met (S108M), Met122 with Ser (M122S) or Ser108 with Met and Met122 with Ser (S108M/M122S) (Figure 2a), and then determined subcellular localization of PsAvh113, PsAvh113$^{\triangle IR1}$, PsAvh113$^{\triangle IR2}$, PsAvh113^{S108M} and PsAvh113^{M122S} in *N. benthamiana* leaves by confocal microscopy (Figure S3a–f). The results showed that, like YFP-PsAvh113 (WT protein), PsAvh113$^{\triangle IR1}$ was uniformly
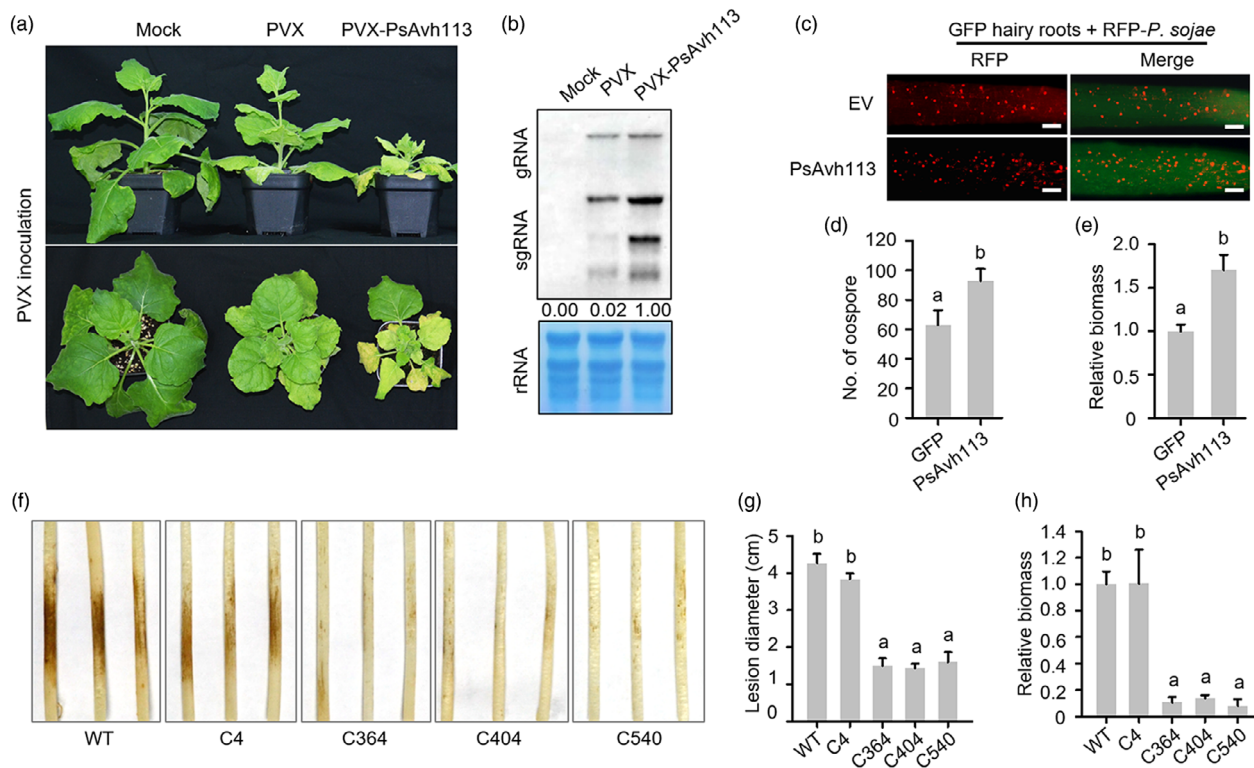
Figure 1 *PsAvh113* is an important virulence factor of *Phytophthora sojae*. (a) Phenotypic comparison of *Nicotiana benthamiana* plants infiltrated with PVX-*PsAvh113*, PVX, or no construct (mock treatment; negative control) at 21 days post-infiltration (dpi). *PsAvh113* expression retarded plant growth and caused leaf yellowing and atrophy. (b) RNA blot showing the accumulation of PVX genomic and subgenomic RNAs at 14 dpi. (c) Oospore production in soybean hairy roots expressing *PsAvh113* or empty vector (EV) and inoculated with RFP-labelled *P. sojae* (RFP-P6497). Scale bars, 0.25 mm. (d) Analysis of the number of *P. sojae* oospores in soybean hairy roots at 48 hpi using a confocal microscope. (e) Quantification of *P. sojae* biomass in soybean hairy roots by qPCR. (f) Comparison of disease symptoms in soybean hypocotyls inoculated with the *PsAvh113*-edited *P. sojae* generated using the CRISPR/Cas9 technology. Pathogen virulence was greatly impaired in soybean hypocotyls. Disease symptoms in etiolated hypocotyls were observed and photographed at 3 dpi. The C4 transformant without *PsAvh113*-editing events was used as a control. (g) Lesion length on soybean hypocotyls upon inoculation with different *PsAvh113* knockout transformants. (h) Relative biomass of *P. sojae* as determined by qRT-PCR. Data represent mean ± standard error (SE). Different letters in (d), (e), (g), and (h) indicate statistically significant differences ($P < 0.01$; Duncan's multiple range test). The experiment was performed in triplicate with similar results.

distributed in the cytoplasm and the nucleus; however, the fluorescence intensity of YFP-PsAvh113$^{\triangle IR2}$ in the nucleus was significantly lower than that of PsAvh113 (Figure S3a–c), suggesting that the IR2 region is associated with the nuclear localization of PsAvh113. Similar to PsAvh113, PsAvh113^{S108M} was uniformly distributed in the cytoplasm and the nucleus, while weak fluorescence was observed in the nucleus of the epidermic cells that expressed PsAvh113^{M122S} (Figure S3d–f), indicating that Met122 residue of PsAvh113 plays a key role in the nuclear localization. Intriguingly, similar to PsAvh113, PsAvh113$^{\triangle IR1}$ induced strong disease symptoms and viral RNA accumulation, whereas PsAvh113$^{\triangle IR2}$ caused slight disease symptoms and lower viral RNA accumulation in the VIVE assay (Figure 2b,c), suggesting that the IR2 region of PsAvh113 is required for PVX infection. Similar results were obtained when *PsAvh113*, *PsAvh113*$^{\triangle IR1}$ and *PsAvh113*$^{\triangle IR2}$ were transiently expressed in soybean hairy roots, and the transformed roots were subsequently inoculated with *P. sojae* (Figure 2d–f). To further explore whether the virulence function of PsAvh113 is due to difference in two amino acid residues, we analysed three residue substitution mutants PsAvh113^{S108M}, PsAvh113^{M122S} and PsAvh113$^{S108M/M122S}$ using

a transient expression system in *N. benthamiana* leaves. Similar to PsAvh113, PsAvh113^{S108M} induced severe disease symptoms and higher viral RNA accumulation, whereas PsAvh113^{M122S} and PsAvh113$^{S108M/M122S}$ caused mild disease symptoms and lower viral RNA accumulation, indicating that both mutants did not completely lose their virulence activity (Figure 2g,h). These results show that the IR2 motif of PsAvh113 is required for its virulence activity and the methionine (M122) of the IR2 region is an important residue for PVX infection.

To evaluate whether the nuclear localization of PsAvh113 is required for virulence, we fused a nuclear export sequence (NES) or nuclear localization sequence (NLS) to the N terminus of PsAvh113, respectively. Confocal imaging showed that NLS-PsAvh113 was exclusively present in nuclei, whereas NES-PsAvh113 was almost completely excluded from the nuclei (Figure S4a). Compared with the YFP control, *N. benthamiana* leaves expressing *NLS-PsAvh113* showed significantly reduced *P. parasitica* resistance, larger lesions and higher pathogen biomass, similar to those expressing *PsAvh113*, whereas leaves expressing *NES-PsAvh113* showed no increase in the severity of disease symptoms (Figure S4b,c). Expression of PsAvh113, NLS-
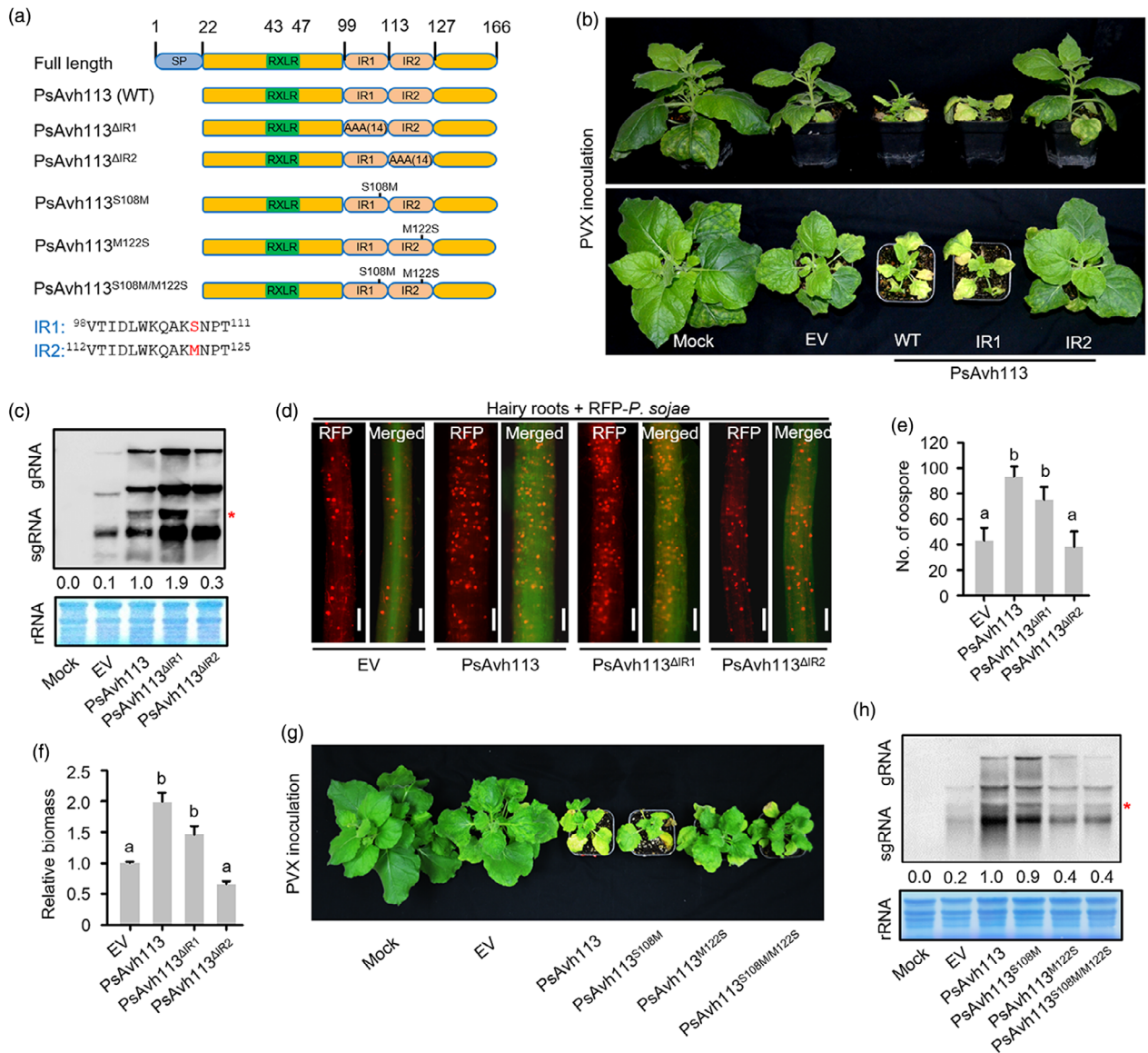
Figure 2 IR2 motif of PsAvh113 plays a crucial role in *Phytophthora* infection. (a) Schematic diagram of full-length (wild-type; [WT]) and mutant versions of PsAvh113. PsAvh113 contains two internal repeats (IR1 and IR2). All residues in the IR region were substituted with alanine residues in the mutant proteins PsAvh113^ΔIR1 and PsAvh113^ΔIR2. The residues in two IR regions showed one amino acid difference, and three mutual substitution mutants of the residues between Ser118 and Met122 were shown. SP, signal peptide. The number above each structure indicates the position of the amino acid. (b) Phenotypic comparison of *N. benthamiana* plants infiltrated with PVX, PVX-*PsAvh113*, PVX-*PsAvh113*^ΔIR1, or PVX-*PsAvh113*^ΔIR2. Plants infected with PVX or PVX-*PsAvh113*^ΔIR2 showed mild disease symptoms. Photographs were taken at 21 dpi. (c) RNA blot showing the accumulation of PVX genomic and subgenomic RNA at 14 dpi. (d) Oospore production in soybean hairy roots expressing *PsAvh113*, *PsAvh113*^ΔIR1, *PsAvh113*^ΔIR2 or EV. Scale bars, 0.25 mm. (e) Oospore count determined at 48 hpi under a confocal microscope. (f) Quantification of *P. sojae* biomass in soybean hairy roots by qPCR. (g) Phenotypic comparison of *N. benthamiana* plants infiltrated with PVX, PVX-*PsAvh113*, PVX-*PsAvh113*^S108M, PVX-*PsAvh113*^M122S or PVX-*PsAvh113*^S108M/M122S. Plants infected with PVX-*PsAvh113*^M122S or PVX-*PsAvh113*^S108M/M122S showed mild disease symptoms. Photographs were taken at 21 dpi. (h) RNA blot showing the accumulation of PVX genomic and subgenomic RNA at 14 dpi. The red asterisk in (c) and (h) represents sgRNA expression that might be caused by *PsAvh113* and its mutants. Data represent mean ± SE. Different letters in (e) and (f) indicate statistically significant differences ($P < 0.01$; Duncan's multiple range test). The experiment was performed in triplicate with similar results.

PsAvh113 and NES-PsAvh113 was confirmed by western blot (Figure S4d). Similar disease symptoms were also observed in the VIVE assay when PsAvh113, NLS-PsAvh113 and NES-PsAvh113 were expressed in *N. benthamiana* leaves (Figure S4e,f). Collectively, these results suggest that the virulence activity of PsAvh113 is dependent on its nuclear localization *in planta*.

PsAvh113 interacts with GmDPB in soybean

To identify the potential host targets of PsAvh113, we performed yeast two-hybrid (Y2H) screening using PsAvh113 as a bait against a soybean cDNA library prepared from *P. sojae*-infected plants. Among the PsAvh113-associated cDNA fragments, yeast cells co-transformed with PsAvh113 and Glyma.01G228100

formed colonies on selection media (Figure 3a). The *Glyma.01G228100* gene, which was repeatedly identified in four independent screens, encodes a putative DPB transcription factor in soybean (Figure S5a). Interestingly, we found that mutation in the nucleotide sequence of IR2, but not in that of IR1, abolished the interaction between PsAvh113 and GmDPB in Y2H assays (Figure 3a). To further examine the direct association between PsAvh113 and GmDPB, we conducted the bimolecular fluorescence complementation (BiFC) assay. PsAvh113, PsAvh113 mutants and GmDPB were fused to the N- and C-terminal halves of the yellow fluorescent protein (YFP; YN and YC), respectively, and the resulting constructs were transformed into *N. benthamiana* leaves in various combination. After 48 h, strong YFP signal was detected in leaf cells co-expressing *YC-GmDPB* and *YN-PsAvh113* or *YN-PsAvh113*^ΔIR1 but not in cells expressing *YC-GmDPB* + *YN-PsAvh113*^ΔIR2, *YC-GmDPB* + *YN* or *YC* + *YN-PsAvh113* (Figures 3b and S5b). To confirm the PsAvh113–GmDPB interaction, we performed a co-immunoprecipitation (co-IP) assay by co-expressing *PsAvh113*, *PsAvh113*^ΔIR1 or *PsAvh113*^ΔIR2 with *GmDPB* in *N. benthamiana* leaves. Total proteins were extracted from the co-infiltrated leaves, and incubated with anti-MYC resin. Immunoblotting with anti-HA antibody revealed that the abundance of PsAvh113-YFP-3*HA and PsAvh113^IR1-YFP-3*HA in the precipitate was high, whereas that of PsAvh113^IR2-YFP-3*HA was low or non-existent (Figure 3c). These results imply that the IR2 region of PsAvh113 mediates its association with GmDPB, and is required for pathogenesis. Furthermore, we generated a mutant variant of GmDPB (GmDPB-M) lacking 86 aa, which is required for its heterodimerization with E2F. In both Y2H and co-IP assays, GmDPB-M was unable to interact with PsAvh113, PsAvh113^ΔIR1 and PsAvh113^ΔIR2 (Figure S5c–e), indicating that region of forming heterodimerization is important for the PsAvh113–GmDPB interacation.

GmDPB enhances plant resistance against *Phytophthora* infection

To investigate the potential role of GmDPB in plant immunity, we firstly overexpressed the *GmDPB* gene in soybean hairy roots and then confirmed GmDPB expression by western blot analysis (Figures 3d and S6). Soybean root tissues transformed with *Agrobacterium* carrying GmDPB or EV were inoculated with RFP-labelled *P. sojae* strain P6497. At 48 hpi, the oospore count in roots overexpressing *GmDPB* was lower than that in roots transformed with the EV control (Figure 3d). Additionally, qPCR analysis showed that the accumulation of *P. sojae* biomass was reduced in the *GmDPB*-overexpressing roots compared with the EV control (Figure 3e). Next, we knocked down *GmDPB* in soybean hairy roots using the CRISPR/Cas9 system. The hairy root lines harbouring nucleotide deletions in the *GmDPB* coding sequence, as determined by Sanger sequencing, were challenged with P6497-RFP (Figure S6b). The *GmDPB*-edited hairy roots displayed increased susceptibility to *P. sojae* infection compared with the control hairy roots (Figure 3f). The oospore count and *P. sojae* biomass were higher in *GmDPB*-edited hairy roots than in hairy roots carrying EV (Figure 3g). These results indicate that GmDPB promotes disease resistance against *P. sojae* in soybean.

To further support the role of *DPB* in plant defence, we performed inoculation assays in *N. benthamiana* and *Arabidopsis*. Consistent with our observations in soybean, *N. benthamiana* leaves overexpressing *GmDPB* were more resistant to *P. parasitica* relative to leaves habouring *YFP* gene (Figure S6c–e), whereas the

AtDPB knockout mutant displayed significantly decreased resistance to *P. parasitica* compared with wild type leaves (Figure S6f–h). Taken together, these results suggest that *DPB* genes promotes disease resistance in *Arabidopsis, N. benthamiana* and soybean.

PsAvh113 induces the degradation of GmDPB *in planta*

To gain insights into the effect of PsAvh113 on GmDPB function, fusions of *PsAvh113-Flag* and its mutated derivatives with *YFP* were co-expressed with *YFP-GmDPB-MYC* in *N. benthamiana* leaves via agroinfiltration. The results exhibited that a lower amount of GmDPB accumulated in the presence of PsAvh113 than in the YFP control, and the degradation of GmDPB was increased with an increasing amount of PsAvh113 (Figure 4a). Immunoblot analysis suggested that PsAvh113^ΔIR1, but not PsAvh113^ΔIR2 affected the reduction of GmDPB protein in co-infiltrated *N. benthamiana* leaves (Figure 4b). Furthermore, the reduced protein of GmDPB can be rescued in *N. benthamiana* leaves coinfiltrated PsAvh113 with GmDPB upon treatment with the proteasome inhibitor MG132 (Figure 4c). Taken together, PsAvh113 causes the degradation of GmDPB by 26S proteasome. These data prompted us to examine where the PsAvh113 degrades GmDPB by 26S proteasome, fusions of PsAvh113 and its mutated derivatives with CFP were co-expressed with -GmDPB-YFP in *N. benthamiana* leaves via agroinfiltration, respectively. Confocal microscopy analysis showed that GmDPB-YFP was primarily appeared in the nucleus and cytoplasm in the absence of PsAvh113 (Figure S6i,j). However, GmDPB-YFP signals were observed in cytoplasm in the presence of PsAvh113-CFP or PsAvh113^IR1-CFP (Figure 4d). Furthermore, similar to that of the EV control, GmDPB-YFP appeared in the nucleus and cytoplasm in the presence of PsAvh113^ΔIR2 (Figure 4d). The percentage of cells expressing GmDPB with EV or together with PsAvh113^ΔIR2 that exhibited clear and strong fluorescence in the nucleus was about 80%, whereas when GmDPB was co-expressed together with PsAvh113 or PsAvh113^ΔIR1, this percentage was decreased to approximately 30% (Figure 4e). Furthermore, western blot analysis was performed using the cytoplasmic and nuclear extracts fractionated from *N. benthamiana* leaves co-expressing PsAvh113-CFP or PsAvh113 mutants -CFP and GmDPB-YFP. Compared with the co-expressing of GmDPB-YFP and CFP in *N. benthamiana* (control), the GmDPB protein in the nuclear fraction and cytoplasm were markedly reduced in presence of CFP-PsAvh113 and CFP-PsAvh113^ΔIR1 (Figure 4f). To further confirm the degradation of GmDPB fusions of NES-PsAvh113, NLS-PsAvh113 or YFP-HA were co-expressed with GmDPB-YFP-HA in *N. benthamiana* leaves via agroinfiltration (Figure S7). Immunoblot analysis suggested that both NES-PsAvh113 and NLS-PsAvh113 affected the reduction of GmDPB protein in co-infiltrated *N. benthamiana* leaves and the reduced protein of GmDPB can be rescued upon treatment with the proteasome inhibitor MG132 (Figure S7), indicating PsAvh113-induced the degradation of GmDPB by 26S proteasome occurs in both the cytoplasm and nucleus. These results indicate that PsAvh113 remarkably inhibits the accumulation of GmDPB protein in nucleus and cytoplasm.

To elucidate whether PsAvh113 affects GmDPB-induced resistant to *Phytophthora*, we co-expressed *GmDPB* with *PsAvh113*, *PsAvh113*^ΔIR1 or *PsAvh113*^ΔIR2 in *N. benthamiana* leaves prior to pathogen challenge. Co-expression of *PsAvh113* or *PsAvh113*^ΔIR1 with *GmDPB* resulted in greater susceptibility to *P. parasitica* than the resistance induced by the expression of
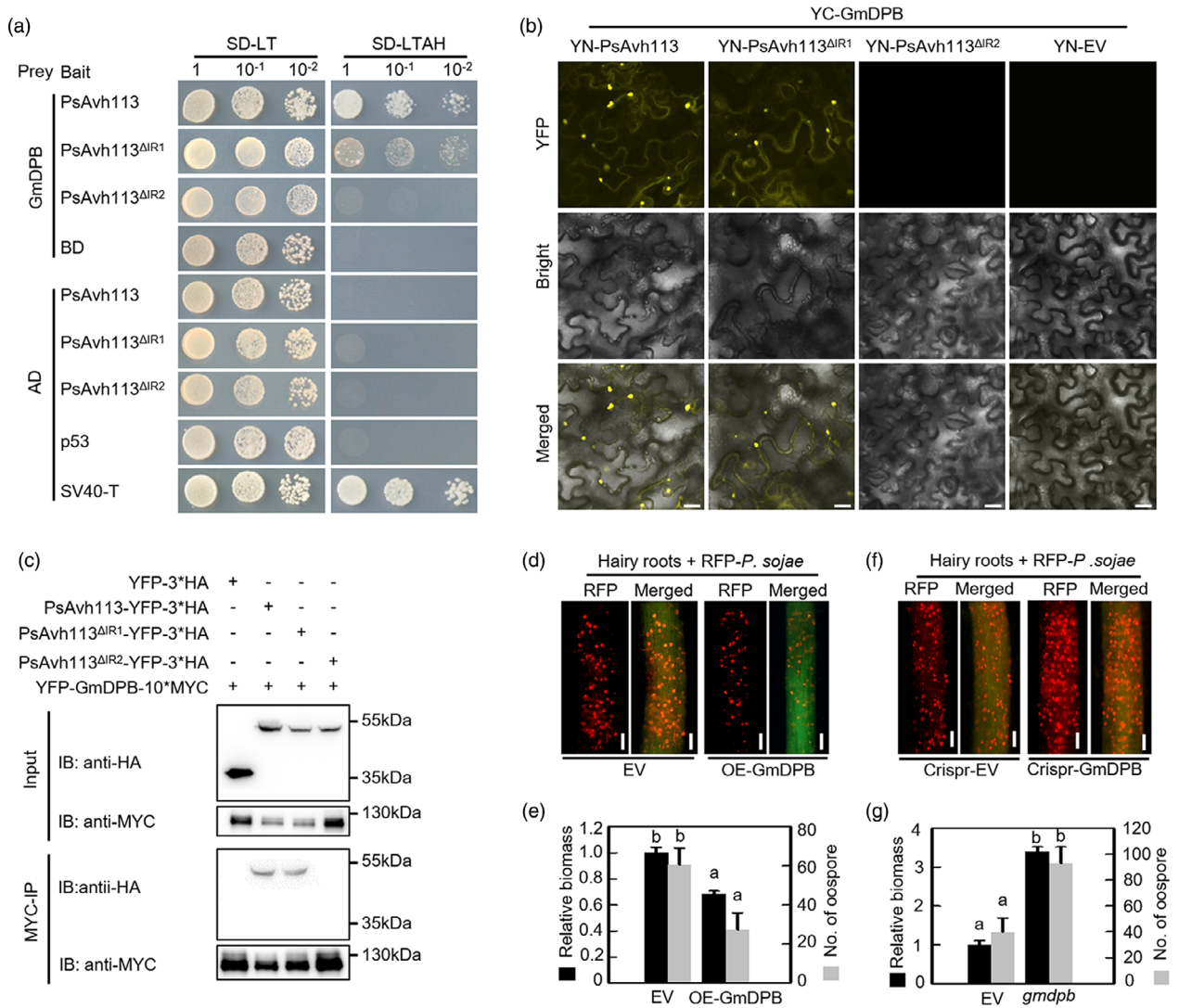
Figure 3 PsAvh113 physically interacts with GmDPB, which acts as a positive regulator of resistance to *P. sojae*. (a) Y2H assay showing that the IR2 domain of PsAvh113 mediates its interaction with GmDPB. The yeast strain AH109 was transformed with the bait plasmid pGBKT7 (BD) carrying *PsAvh113*, *PsAvh113^ΔIR1* or *PsAvh113^ΔIR2* together with the prey plasmid pGADT7 (AD) carrying *GmDPB*. Transformants were selected on minimal medium. SV40-T and p53 were used as a positive control combination. -TL and -TLHA indicate SD/-Trp-Leu and SD/-Trp-Leu-His-Ade plates, respectively. Colony formation on -TLHA plates indicates an interaction between the two proteins. (b) BiFC assay showing the interaction between PsAvh113 or PsAvh113 mutants and GmDPB. (c) Co-IP assays showing that PsAvh113 and PsAvh113^ΔIR1 interact with GmDPB, whereas PsAvh113^ΔIR2 does not. Total proteins were extracted from *N. benthamiana* leaves expressing *YFP-GmDPB-10*MYC* and *PsAvh113-YFP-3*HA* or YFP-3*HA-tagged *PsAvh113^ΔIR1* or *PsAvh113^ΔIR2*. Immune complexes were pulled down using anti-MYC agarose gel. Proteins that co-precipitated with GmDPB were detected by western blotting. (d–g) Confocal microscopy analysis (d, f) and quantification (e, g) of oospores and pathogen biomass in soybean hairy roots overexpressing WT, *GmDPB* (d, e) or edited *GmDPB* (f, g) along with the EV control. Scale bars, 0.25 mm. Confocal microscopy analysis was conducted at 48 hpi. In (e) and (g), black columns represent pathogen biomass, and grey columns represent oospore count. Data represent mean ± SE. Different letters in (e) and (g) indicate statistically significant differences (*P* < 0.01; Duncan's multiple range test). The experiment was performed in triplicate with similar results.

GmDPB alone (Figure 4g,h). This inhibiting effect was not observed when *PsAvh113^ΔIR2* was used in place of *PsAvh113* for co-expression with *GmDPB* (Figure 4g,h). Taken together, the results suggest that PsAvh113 decreases the stability of GmDPB, leading to increased *Phytophthora* infection.

GmDPB functions as a transcriptional activator of *GmCAT*

A previous study showed that DPB binds to the GCGGGAA motif in the promoter of target genes in human (Cheneby *et al.*, 2018). Interestingly, we detected two cis-elements within ~1.5 kb region

upstream of the coding sequence of *GmCAT1* (*Glyma.14G223500*) using the PLACE program (Higo *et al.*, 1999) (Figure S8a,b). There are four *CAT* genes in soybean, but the GCGGGAA motif was not detected in promoter region of other three *CAT* genes (Figure S8c). The GmCAT1 protein is localized to the peroxisomes (Figure S8d). To determine whether GmDPB binds to the promoter of *GmCAT1*, we performed yeast one-hybrid (Y1H) assays. Our results showed that GmDPB fused to the GAL4 transcriptional activation domain (AD) activated the expression of the AbA reporter gene driven by the *GmCAT1* promoter (Figure 5a). Moreover, we analysed the promoter

regions of one allele, *GmCAT2*, and found that the *GmCAT2* promoter has no GCGGGAA motif, supporting the notion that GmDPB was unable to bind to *GmCAT2* promoter in the Y1H assay (Figure 5a). Next, we performed a transactivation assay in *N. benthamiana* leaves using the *LUC* reporter construct, which contained four tandem copies of the cis-elements of the *GmCAT1* promoter, and the *GmDPB* effector construct, and showed that GmDPB acts as a transcriptional activator (Figure 5b). Subsequently, we performed an EMSA using the purified MYC-tagged GmDPB protein along with the Cy3-labelled double-stranded oligonucleotide probe (Table S1). In the presence of GmDPB, the probe showed a shift in its position and migrated more slowly than the free probe; however, this shift was not observed in the presence of EV (Figure 5c), suggesting that GmDPB binds to the GCGGGAA motif. Consistent with these results, the transcript level of *GmCAT1* was significantly up-regulated in *GmDPB*-overexpressing hairy roots but markedly down-regulated in *GmDPB*-edited lines compared with EV (Figure 5d,e).

PsAvh113 represses the DNA-binding activity of GmDPB both *in vitro* and *in vivo*

To examine the regulatory effect of GmDPB on the expression of its target genes, we performed transient expression assays in soybean hairy roots by expressing the *GUS* reporter gene under the control of a 1.8 kb fragment of the *GmCAT1* promoter. When the reporter construct (*pGmCAT1:GUS*) and control construct (*p35S:GUS* or *p35S:GFP*) were co-transformed into soybean hairy roots, we detected GUS activity driven by the *GmCAT1* promoter or by *35S* promoter (*p35S:GUS*) as the positive control (Figure 5f). In addition, GUS staining was weaker at the tip of hairy roots expressing the *GmCAT1* promoter together with *PsAvh113* than that together with *GFP* (Figure 5f). To determine whether PsAvh113 affects the GmDPB-induced expression of *GmCAT1*, we examined the DNA-binding ability of GmDPB in the presence of PsAvh113 by performing an EMSA assay. Interestingly, we found that the DNA-binding ability of GmDPB was reduced by PsAvh113 in a dose-dependent manner, but not by PsAvh113[ΔIR2] (Figures 5g and S8e), indicating that PsAvh113 inhibits the DNA-binding activity of GmDPB through its IR2 motif *in vitro*.

Next, we analysed the expression of *GmCAT1* during *P. sojae* infection in soybean. The transcript level of *GmCAT1* was significantly induced in soybean plants inoculated with the *PsAvh113* knockout mutant compared with those infected with the WT strain P6497 (Figure 5h). However, the expression of *GmCAT2* showed no change or slight reduction in soybean when inoculated with the *PsAvh113* knockout mutant compared with those infected with the WT strain P6497 (Figure S8f). Meanwhile, the transcript levels of *GmCAT1* were down-regulated in hairy roots expressing *PsAvh113* or *PsAvh113[ΔIR1]* compared with roots carrying EV or *PsAvh113[ΔIR2]* (Figure 5i). Finally, we tested the expression of *AtCAT* in *Arabidopsis* transgenic lines expressing *PsAvh113*, and the results obtained were similar to those in soybean (Figure S8g). Taken together, these results indicate that PsAvh113 affects the stability of GmDPB and the DNA-binding activity of the encoded protein, thereby disrupting *GmDPB*-regulated functions of the downstream gene *GmCAT1*.

GmCAT1 contributes to resistance against *Phytophthora* pathogens

Our finding that *GmCAT1* is the potential target of GmDPB led us to further investigate its biological roles in plant defence. To

understand the potential role of GmCAT1 in soybean, we expressed the *GmCAT1* gene in soybean hairy roots and found that *GmCAT1* was strongly increased at the transcriptional level (Figures 6a and S9a). Upon P6497-RFP inoculation, fewer oospores were produced in *GmCAT1*-overexpressing roots compared with hairy roots expressing EV (Figure 6b). Compared with that expressing empty vector control, the results of qPCR analysis showed decreased accumulation of *P. sojae* biomass in *GmCAT1*-overexpressing hairy roots (Figure 6b). Furthermore, to edit the *GmCAT1* gene, we designed two gRNAs including gRNA1, which targeted the GmDPB-binding site in the *GmCAT1* promoter (pGmCAT1), and gRNA2, which targeted the coding sequence of *GmCAT1*, and performed genetic transformation of HC6 hairy roots (Figure S9b). Compared with the EV control, the *GmCAT1* or p*GmCAT1*-edited hairy roots exhibited stronger disease symptoms upon *P. sojae* infection, as indicated by the increased oospore count and biomass (Figure 6c,d), suggesting that *GmCAT* suppresses the progression of *P. sojae* infection in soybean. The expression of *GmCAT1* was reduced in p*GmCAT1*-edited and *GmCAT1*-edited hairy roots (Figure 6e).

These findings prompted us to test whether *GmCAT1* is involved in programmed cell death in plants. We firstly assessed the PsAvh113 using a transient expression assay in *N. benthamiana* and found that both PsAvh113 and PsAvh113[ΔIR2] did not trigger cell death (Figures 6f and S9c,d). Similar to Avr1b, PsAvh113 suppresses Bax-induced cell death in *N. benthamiana* leaves, while PsAvh113[ΔIR2] fails to inhibit cell death which is comparable to EV (Figure 6f). Furthermore, GmDPB is not able to induce cell death and also cannot inhibit Bax-induced cell death (Figure 6g). Interestingly, GmCAT1 induces slightly PCD, whereas the GmCAT1-induced cell death is blocked by PsAvh113 alone or PsAvh113 together with GmDPB (Figure 6g). Overall, our data showed that GmCAT1 positively regulates plant resistance to *Phytophthora* pathogens, which is likely due to GmCAT1−triggered cell death. Subsequently, this enhanced resistance of GmCAT1 is inhibited by PsAvh113 during *P. sojae* infection, thereby increasing soybean susceptibility to *Phytophthora*.

Discussion

Many efforts have been made to identify virulence factors required for pathogen colonization and disease development, and to elucidate the molecular mechanisms of microbial pathogenicity. However, most virulence effectors have not been characterized in *Phytophthora* pathogens. In this study, we exploited a newly developed screening assay, VIVE (Shi *et al.*, 2020), and successfully identified PsAvh113 as a potential virulence effector in *P. sojae*, which was responsible for growth stunting and severe viral symptoms in *N. benthamiana* plants. Subsequently, using PsAvh113 as a molecular bait, we identified the *GmDPB* gene as its target, thereby providing mechanistic insights into the virulence function of PsAvh113 and the development of PRSR.

During evolution, IR regions may appear within a protein, which play an important role in protein stability and function as well as genome evolution (Jorda and Kajava, 2010). For example, the genome of *Ustilago maydis* encodes 15 effector proteins containing IRs (Mueller *et al.*, 2008); *Mycosphaerella graminicola* genome harbours 23 genes predicted to encode surface-associated proteins possessing tandem IR regions (Rudd *et al.*, 2010); and *Aspergillus fumigatus* genome contains 292 genes with IRs (Levdansky *et al.*, 2007). These repeat motifs are

usually highly variable in size, mainly because of homologous recombination or slippage during replication (O'Dushlaine et al., 2005). Variations in repeat lengths and numbers increase functional diversity and allow adaptation to environmental changes or escape from host immunity (Ma et al., 2018). Our data revealed that the PsAvh113 protein harbours two IR regions

(IR1 and IR2), both of which differ by only a single amino acid residue. Our results show that IR2, but not IR1, is required for the virulence activity of PsAvh113 and for its interaction with GmDPB. And the methionine (M122) of IR2 region is an important residue for PVX infection. This is largely different from another oomycete effector PsAvh23, in which contains two IRs; however, unlike the
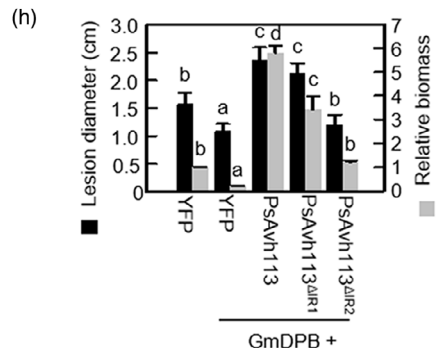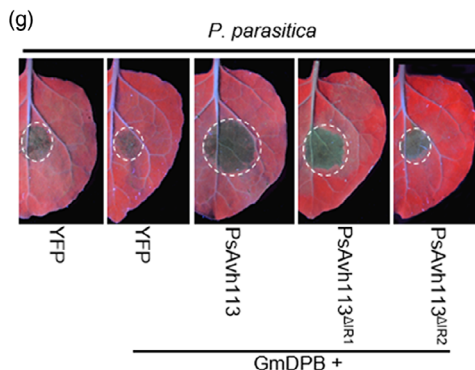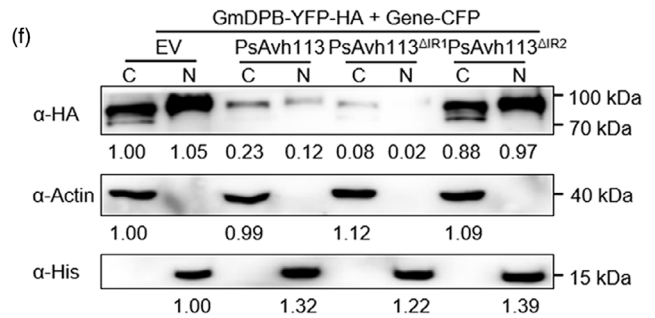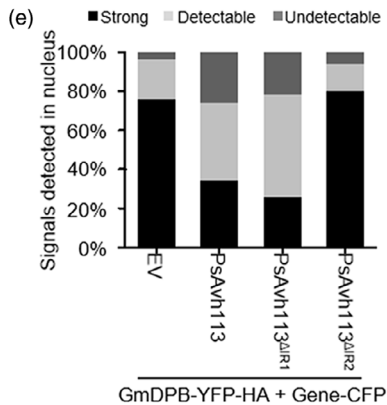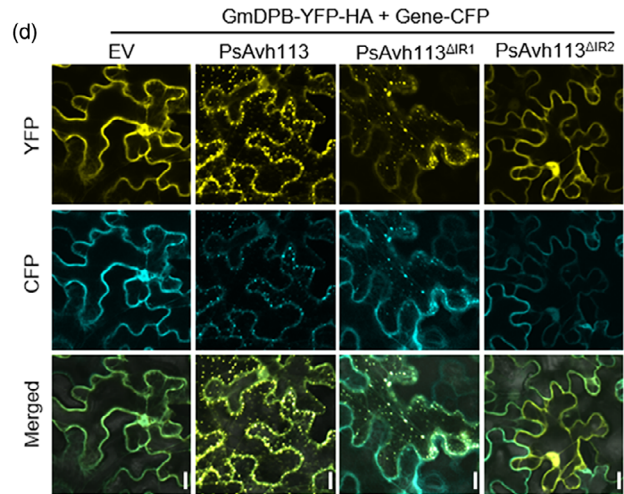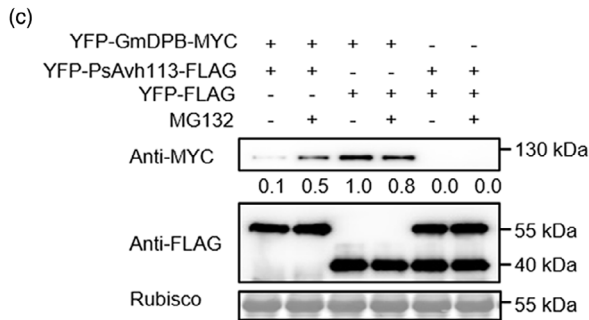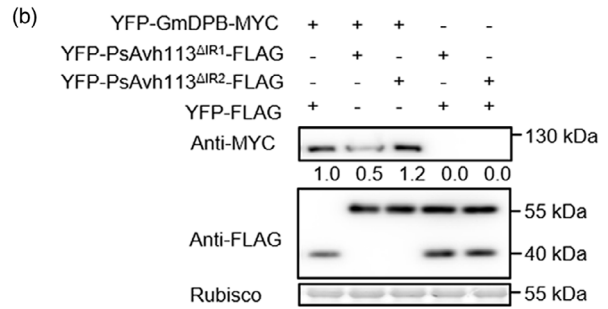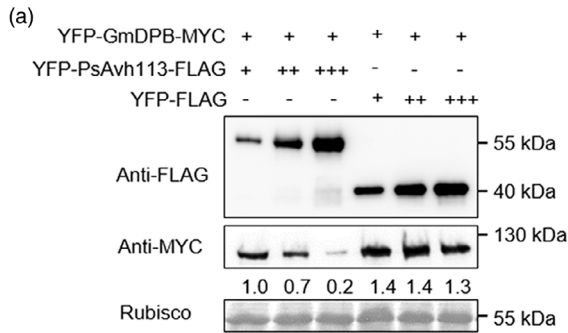
Figure 4 PsAvh113 affects the stability of GmDPB protein. (a) Western blot showing that co-expression of *GmDPB* with *PsAvh113* reduces GmDPB abundance, and PsAvh113 affects the stability of GmDPB in a dose-dependent manner. (b) Western blot showing that co-infiltration of *GmDPB* with *PsAvh113^ΔIR1*, but not *PsAvh113^ΔIR2*, reduces GmDPB abundance, and IR2 motif of PsAvh113 associataes with affects the stability of GmDPB in *N. benthamiana*. (c) Western blot displaying that the degradation of GmDPB protein was prevented by application of proteasome inhibitor MG132 in *N. benthamiana* leaves co-expressed *GmDPB* with *PsAvh113*. (d) Subcellular localization of CFP-tagged WT and mutant PsAvh113 proteins and YFP-HA-labelled GmDPB in *N. benthamiana* leaves upon agroinfiltration. Fluorescence was detected by confocal microscopy at 48 hpi. Scale bars, 40 μm. (e) A total of 50 epidermal cells of *N. benthamiana* expressing GmDPB-YFP-HA alone, GmDPB-YFP-HA together with PsAvh113 or PsAvh113 mutants, respectively, were screened for the distribution of fluorescence. The strong means a strong signal in the nucleus, the detectable means a partial signal in nucleus and the undetectable means no signal in the nucleus. (f) Western blot analysis of GmDPB-YFP-HA in cytoplasmic and nuclear extracts from *N. benthamiana* leaves. The cytoplasmic and nuclear fractions were analysed of GmDPB-YFP-HA with PsAvh113 or PsAvh113 mutants by western blot with anti-HA antibody, and GmDPB-YFP-HA with CFP was used as control. Actin and histone H3 were detected as fractionation markers for the cytoplasm and the nucleus, respectively. (g) Disease symptoms on *N. benthamiana* leaves co-expressing the indicated constructs. Leaves were detached from the plants and inoculated with *P. parasitica*. Disease symptoms were monitored and photographed under ultraviolet (UV) light at 2 dpi. (h) qRT-PCR analysis of relative *Phytophthora* biomass (grey columns) and *P. parasitica* lesion size (black columns) of 15 infected leaves were counted at 48 hpi. Data represent mean ± SE. Different letters indicate statistically significant differences ($P < 0.01$; Duncan's multiple range test). The experiment was performed in triplicate with similar results.

IRs in PsAvh113, both IRs in PsAvh23 are responsible for its virulence activity and interaction with the ADA2 subunit of the histone acetyltransferase complex (Kong *et al.*, 2017), indicating that oomycete pathogens have also evolved effectors harbouring different IRs to suppress host immunity, the biological function of IR1 in PsAvh113 needs further investigations by protein crystal structure in the future.

The E2F/DP family of transcription factors is widely believed to play a pivotal role in regulating cell cycle progression, DNA replication, DNA damage repair and stress response (Perrot-Rechenmann, 2010; Wang *et al.*, 2014). In animals and plants, the E2F/DP family includes typical E2Fs and their related dimerizing partners, called DP proteins, both of which hetero-dimerize to bind to the E2F site in the promoters of target genes (Kosugi and Ohashi, 2002b). Because DP proteins function as essential DNA-binding partners of E2Fs, most of the previous studies focused on how DP proteins enhance the transcriptional activation or repression of E2F target genes, and the self-regulatory roles of DP protein have not been fully explored. In the present study, we showed that the *GmDPB* positively regulates the host immune response to *Phytophthora* pathogens, and acts as the direct host target of PsAvh113. Moreover, upon binding, nuclear signals of GmDPB were tough to detect in epidermal cells of *N. benthamiana* leaves. In addition, there was a modest increase in the decay rate of GmDPB in the presence of PsAvh113, indicating that the PsAvh113-induced punctate localization in the cytoplasm is detrimental for the stability of GmDPB. Our findings are in agreement with previous results showing that the tumour suppressor protein ARF binds to and induces the nucleolar relocalization of DP1, leading to the inhibition of E2F-activated genes (Datta *et al.*, 2005). More interestingly, we observed that GmDPB-M, which lacked the region important for heterodimerization with E2Fs, also failed to associate with PsAvh113. This prompted us to examine whether GmDPB associates with PsAvh113 either through GmE2Fs, or PsAvh113 and GmE2F independently bind GmDPB through the heterodimerization domain in the future. The latter would suggest the possibility that GmE2Fs and PsAvh113 compete with each other to bind to GmDPB.

Our results showed that GmDPB functions as a transcription activator of *GmCAT1* by binding to its promoter. Furthermore, PsAvh113-mediated inhibition of *GmDPB* activity reduced the expression of *GmCAT1*. Plant CAT, as a type of peroxisomal enzyme, plays crucial roles in maintaining H_2O_2 homeostasis and

regulating PCD (Mhamdi *et al.*, 2010; Zhang *et al.*, 2015). In the present study, *GmCAT1* could slightly induce cell death in *N. benthamiana* and positively regulated disease development by *P. sojae*. Analogous to from RxLR effector, analysis of CRN (crinkling- and necrosis-inducing proteins) effectors showed that the PsCRN63 effector induces cell death, while PsCRN115 suppresses cell death in *N. benthamiana* leaves (Liu *et al.*, 2011). Subsequently, PsCRN63/115 effectors regulate plant PCD through directly interfering with CATs, and perturbing H_2O_2 homeostasis, thereby, overcoming plant immune response in *N. benthamiana* (Zhang *et al.*, 2015). These data suggested that *P. sojae* have evolved two different types of effector proteins and distinct mechanism to assault the similar immune-related protein, and ensured *P. sojae* infection and PRSR disease development in soybean. However, the relationship among these effectors remains unknown, which might be a key point for further investigation. Moreover, similar to PsAvh113 of *P. sojae*, an effector PstGSRE1 from Puccinia striiformis f. sp. tritici has been shown to interact with and disrupt the nuclear localization of transcription factor TaLOL2 and suppress ROS-mediated cell death induced by TaLOL2, thus promoting stripe rust of wheat (Qi *et al.*, 2019). Compared to three *CAT* genes in arabidopsis, there are four *CAT* genes in soybean, all of which form one clade and are close to *AtCAT2*. Intriguingly, *GmCAT1* and *AtCAT2* showed differential plant defence responses to pathogens, this is probably due to infection with biotrophic and necrotrophic pathogens (Cheng *et al.*, 2018; Dat *et al.*, 2003; Mur *et al.*, 2006; Yuan *et al.*, 2017; Zhang *et al.*, 2015). We also do not rule out that soybean catalases have distinct functions in catalysing H_2O_2, the precise mechanism of GmCAT1 remains elusive and needs further investigation. Taken together, it is conceivable that a virulence effector of *P. sojae* associates with a host factor and alters its stability, subsequently, inhibits the GmCAT1-induced cell death and leads to disease symptoms during infection (Figure 7). In conclusion, our results indicate that the PsAvh113–GmDPB–GmCAT1 interaction serves as a potential defence mechanism, probably in favour of *P. sojae* infection.

Experimental procedures

Plants and microbe growth conditions

Arabidopsis and *N. benthamiana* plants were grown in a greenhouse (25 °C, 67% relative humidity, 16 h light photoperiod). pEG101-*PsAvh113* was introduced into *Arabidopsis*
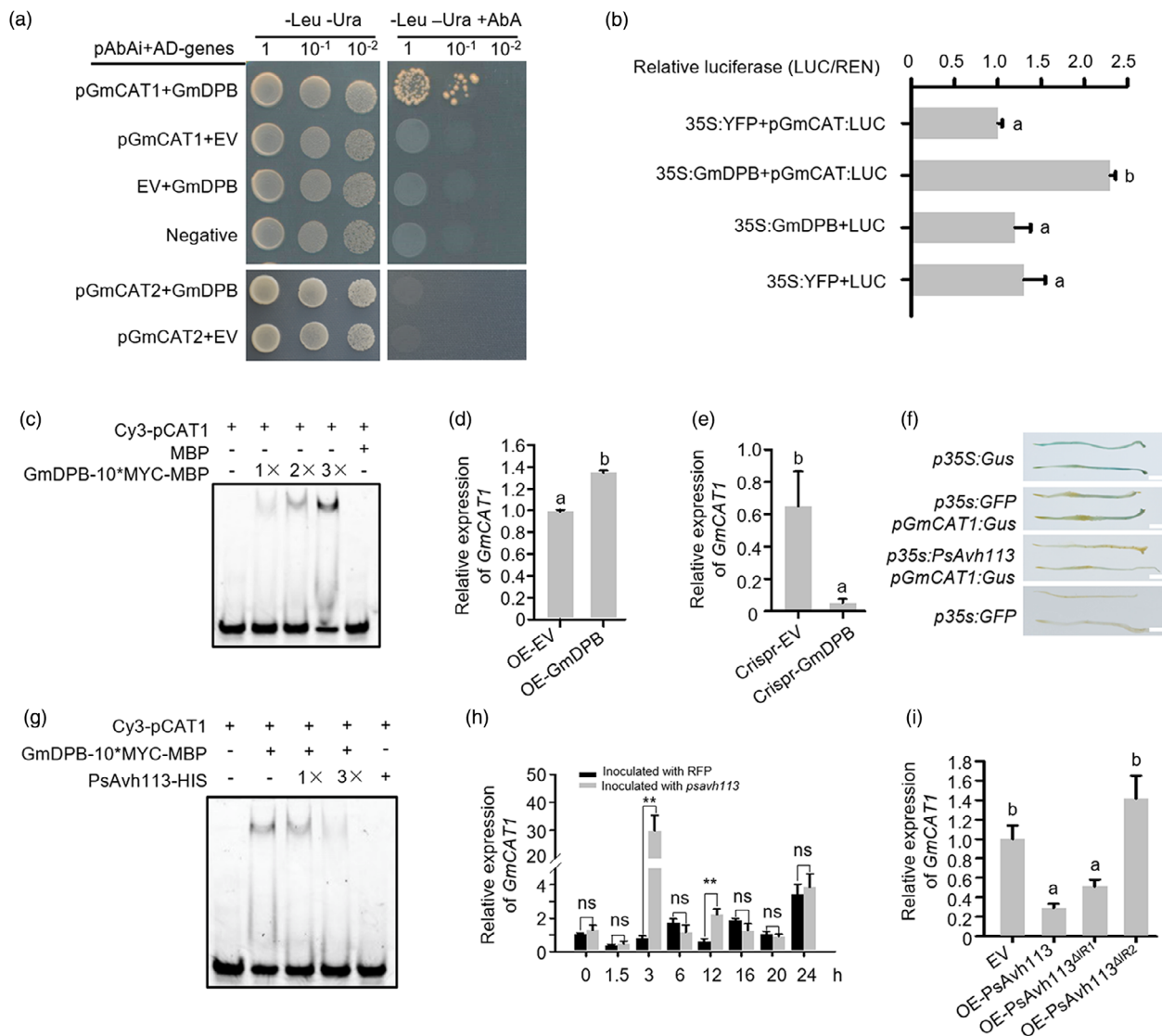
Figure 5 GmDPB specifically binds to the promoter of *GmCAT1* to activate gene expression. (a) Y1H assay showing that GmDPB binds to the *GmCAT1* promoter, but not to the *GmCAT2* promoter. The yeast strain Y1H Gold was co-transformed with the *pGmCAT*-containing pAbAi bait plasmid and AD-GmDPB. Yeast transformants were selected on minimal medium containing 150 ng/mL AbA. (b) Dual luciferase assay showing that GmDPB induces *GmCAT1* expression in *N. benthamiana* leaves. (c) Verification of the binding of GmDPB to the *GmCAT1* promoter via EMSA. The DNA-binding ability of GmDPB increased with its increasing amount. (d) Expression analysis of *GmCAT1* in *GmDPB*-overexpressing soybean hairy roots by qRT-PCR. (e) *GmCAT1* expression is inhibited in *GmDPB*-edited soybean hairy roots, as examined by qRT-PCR. (f) PsAvh113 represses the *GmCAT1* promoter activity in 20-day-old soybean hairy roots treated with *P. sojae* oospores for 48 h. *PsAvh113* and *pGmCAT* were transiently co-expressed in soybean hairy roots, which were then subjected to the GUS staining assay. Scale bars, 4 mm. (g) Verification of the association between PsAvh113 and *pGmCAT1* by EMSA. The binding capacity decreased with the increase in PsAvh113 concentration. (h) Expression profiles of *GmCAT1* in soybean hairy roots inoculated with the P6497 (WT) strain and *PsAvh113* knockout line of *P. sojae*. Asterisks indicate significant differences according to Student's *t*-test ($**P < 0.01$, ns, no significant difference). (i) Analysis of *GmCAT1* transcript levels in soybean hairy roots overexpressing *PsAvh113*, *PsAvh113^ΔIR1* or *PsAvh113^ΔIR2*. Data represent mean ± SE. Different letters in (b), (d), (e) and (i) indicate statistically significant differences ($P < 0.01$; Duncan's multiple range test). Experiments were repeated twice with similar results.

ecotype Col-0 to generate transgenic *Arabidopsis* plants using dipping method. The hairy roots are generated from soybean cotyledons by *Agrobacterium rhizogenes*-mediated transformation. The *P. parasitica* isolate PBS042 and the *P. sojae* isolate P6497 were grown on 10% (v/v) V8 juice agar in the dark at 25 °C. *Agrobacterium tumefaciens* strains GV3101 and *A. rhizogenes* strains K599 were cultured on LB medium supplemented with appropriate antibiotics at 28 °C. *Escherichia coli* strains *Rosetta* and *DH5α* were cultured on LB medium at 37 °C

supplemented with appropriate antibiotics. Given that *Arabidopsis* CAT mRNA abundance is controlled by the circadian clock. In order to avoid the effect of circadian rhythm on expression of soybean *CAT* genes, the sampling time is set to 2 : 00–4 : 00 PM for those plants that are grown in a greenhouse.

Yeast one/two-hybrid assays

The yeast one-hybrid assay was performed to examine DNA-Protein binding using the Gold yeast one-hybrid system (Liu
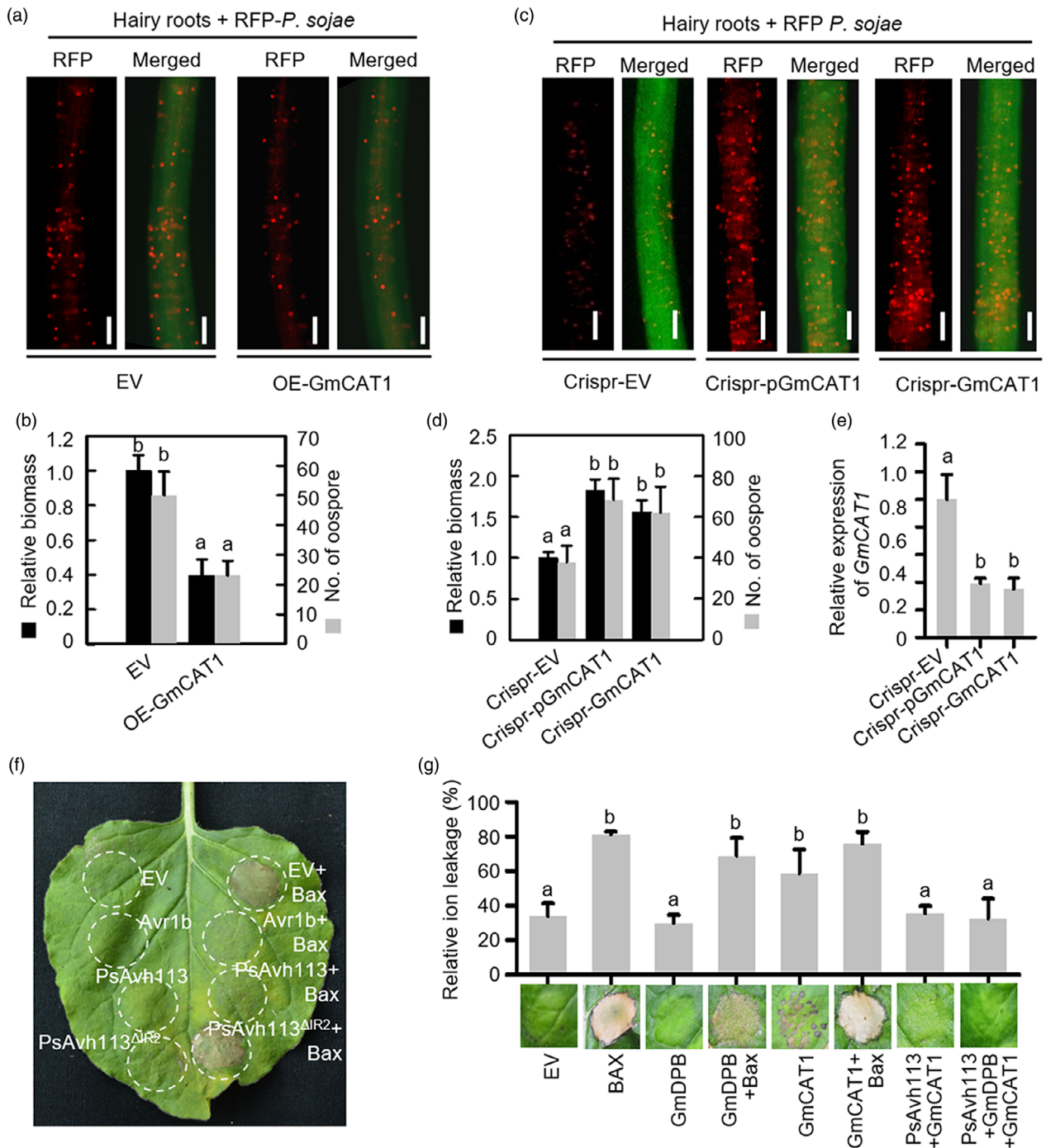
Figure 6 PsAvh113 inhibits the positive immune regulator *GmCAT1*-induced cell death. (a–d) Confocal microscopy analysis (a, c) and quantification (d) of oospores and pathogen biomass in soybean hairy roots overexpressing WT *GmCAT1* (a, b) or edited *GmCAT1* (c, d) along with the EV control. Scale bar, 0.25 mm. Confocal microscopy analysis was conducted at 48 hpi. In (b) and (d), black columns represent biomass, and grey columns represent oospore count. (e) The transcript levels of *GmCAT1* in *GmCAT1*-edited hairy roots. In (b–e), data represent mean ± SE, and different letters indicate statistically significant differences (*P* < 0.01; Duncan's multiple range test). (f) Overexpression of PsAvh113 in *N. benthamiana* suppresses Bax-triggered cell death. *N. benthamiana* leaves were infiltrated with *A. tumefaciens* containing PVX-PsAvh113, PVX-PsAvh113^{ΔIR2}, PVX, or PVX-Avr1b, either alone or with *A. tumefaciens* cells carrying PVX-Bax, which were infiltrated 24 h later. EV, empty vector. (g) *GmCAT1* induces cell death in *N. benthamiana* leaves, whereas overexpression of PsAvh113 in *N. benthamiana* suppresses PCD triggered by *GmCAT1*. Pictures were taken at 5 dpi. Experiments were repeated three times with similar results.

et al., 2019). A 300 bp promoter fragment of *GmCAT1* containing GCGGGAA box (as p*GmCAT1*) was cloned into the pAbAi vector. The CDS of *GmDPB* was inserted into the pGADT7 vector

(AD-GmDPB). The resultant constructs and empty vector pGADT7 were co-transformed into the p*GmCAT* reporter strain by PEG/LiAc yeast transformation method, respectively. The transformed
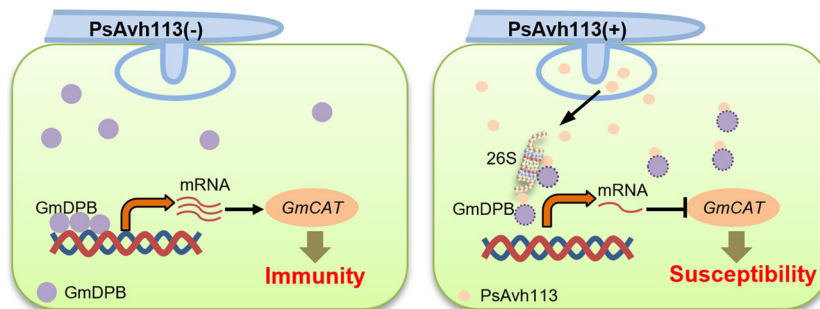
Figure 7 Proposed model demonstrating the role of PsAvh113 in regulating plant immunity. The PsAvh113 virulence effector of *P. sojae* interacts with GmDPB to manipulate *GmCAT1* expression, which eventually leads to PRSR. During *P. sojae* infection, PsAvh113 interacts with the GmDPB transcription factor, affecting its stability. The degradation of GmDPB reduced the ability of binding to the promoter *GmCAT1*, thereby directly inhibiting its expression and activity. Subsequently, the reduced expression of *GmCAT1* decreases PCD triggered by itself and enhances the susceptibility to *P. sojae* in soybean.

colonies were plated on SD/−Leu/-Ura medium containing 1.5 mg/mL Aureobasidin A (AbA) to observe yeast growth. An empty reporter vector was used as a negative control. Y2H assay was carried out as previously described (Gui *et al.*, 2022; Zhang *et al.*, 2019).

Recombinant protein expression and purification

The plasmid pMAL-*GmDPB* that contains the His-tag was transformed into the *E. coli* strain *Rosetta*. To obtain the fusion protein, *Rosetta* cells harbouring the pMAL-*GmDPB* construct were cultured in LB liquid medium supplemented with Ampicillin at 37 °C for 2 h and then induced by 0.5 mM IPTG at 16 °C for 18 h. The induced *Rosetta* cells were sonicated until the solution became clear. The supernatant was collected by centrifugation, and the recombinant proteins were purified using an Ni$^+$-NTA beads.

Electrophoretic mobility shift assay (EMSA)

The His-tagged recombinant constructs (His-GmDPB, His-PsAvh113) were introduced in *E. coli* Rosetta and purified as described above (Cheng *et al.*, 2018; Del Pozo *et al.*, 2007). DNA fragments were end-labelled with Cy3. The fluorescence-labelled DNA (2 pM) was incubated with different amount of purified protein in 30 μL binding system (10 mM Tris–HCl, pH 8.8, 100 mM KCl, 1 mM EDTA, 0.1 mM DTT, 1.5 mM BSA and 5% glycerol) at 25 °C for 30 min. Then 10 × DNA loading buffer was added to the reaction. For DNA competition assays, 10-fold non-labelled competitor DNA was also added to the reaction. For protein competition assays, 10-fold His-PsAvh113 was added in the reaction. The reaction mixture was electrophoresed at 4 °C on an 8% native polyacrylamide gel in 0.5 × TBE (45 mM Tris, 45 mM Borate, 1 mM EDTA) solution for 100 min at 100 V in the dark. Fluorescence-labelled DNA on the gel was directly detected with Amersham Typhoon.

DAB staining assays

Hydrogen peroxide (H$_2$O$_2$) in soybean hairy roots was detected by staining with 3,3′-diaminobenzidine (DAB) tetrahydrochloride hydrate (Cheng *et al.*, 2018). The hairy roots infected by *A. tumefaciens* carrying the construct of overexpression or silencing of targeting gene were harvested at 0 and 48 h after inoculation. The samples were immersed in DAB solution (1 mg/mL, pH 3.8) overnight at room temperature and then were treated using transparent solution (100% Trichloroacetaldehyde) for observation.

Agrobacterium-mediated transformation in soybean hairy roots and *N. benthamiana*

Gene overexpression and knockdown in soybean hairy roots were performed as previously described (Zhang *et al.*, 2019). Briefly, soybean cotyledons were collected and transformed with the overexpression vector (pFGC5941, pBI121 or pBI101) and CRISPR vector (pGES201) that contained interesting gene or fragment using *A. rhizogenes* K599. The treated cotyledons were sealed and placed in a greenhouse at 25 °C. After 3–4 weeks, transformed hairy roots were used to conduct the relative experiments. For transient expression analysis, *N. benthamiana* leaves were transformed by *A. tumefaciens* GV3101 as described previously with minor modification (Qiao *et al.*, 2013). For stabilization assays, protesome inhibitor MG132 was infiltrated into plant leaves that coexpressed *PsAvh113* and *GmDPB* after the agroinfiltration for 24 h.

Histochemical GUS assay

The transcriptional activity was performed as previously described (Mao *et al.*, 2020). The hairy roots were co-transformed with *A. rhizogenes* containing pFGC5941-*GmDPB* and pBI101-*pCAT1* with or without PsAvh113. Hairy roots with pBI121-35S::GUS or *p35s:GFP* were transformed separately. The hairy roots were collected and soaked in GUS Buffer (20 mg/mL X-Gluc, 10 mM Na$_2$EDTA, 100 mM Na$_2$H$_2$PO$_4$, 0.5 mM K$_3$[Fe(CN)$_6$], 0.5 mM K$_4$[Fe(CN)$_6$]·3H$_2$O, 0.1% Triton-X-100, pH 7.0). Following staining for 2 days at 25 °C, the samples were washed in 95% (v/v) ethanol and then photographed.

Dual-luciferase reporter assay

LUC and REN luciferase activity was detected using a dual-luciferase reporter assay system (Promega, USA) on Glomax machine (Promega, USA) as previously described (Iglesias-Ara *et al.*, 2018). Briefly, the effector construct pEG101-*GmDPB* and reporter construct pGreen-p*GmCAT1* were introduced into *Agrobacterium* strain GV3101 separately and then expressed in tobacco leaves by *A. tumefaciens*-mediated transient transformation. Leaf samples were collected and ground to powder at 4 °C separately. Luciferase Assay Substrate was resuspended in Luciferase Assay BufferII to generate LARII and 50 × Stop Glo substrate was added into Stop Glo Buffer to generate Stop Glo Reagent. After measuring firely luciferase activity, 20 μL Stop Glo Reagent was added into the mix to Renilla luciferase activity.

The firefly LUC activity was normalized to the REN activity. The experiment was replicated three times independently.

Real-time quantitative PCR

Leaf discs were sampled from the infected leaves of *N. benthamiana*, *Arabidopsis* or soybean 2 dpi upon *P. parasitica* or *P. sojae* inoculations. An equal amount of samples were used to extract genomic DNA using a genomic DNA isolation kit (TIANGEN BIOTECH, Beijing). *Phytophthora* biomass in inoculated leaves was determined by quantitative PCR (qPCR) using *Phytophthora*-specific primers (Table S1).

For analysis of gene expression, RNA was extracted using TRIzol Reagent (Thermo) according to the manufacturer's instructions. A 1-μg aliquot of total RNA was reverse-transcribed by priming with oligo (dT18) in a 20-μL reaction volume using the HiScript II 1st Strand cDNA Synthesis Kit (+gDNA wiper) (Vazyme Biotech). PCR amplification was conducted using gene-specific primers as previously described (Gui *et al.*, 2022). qRT-PCRs were performed on Lightcycler 480II (Roche) using a ChamQ Universal SYBR qPCR Master Mix Kit (Vazyme, Nanjing, China).

Phytophthora infection assays

Arabidopsis was infected with *P. parasitica* as described before (Zhu *et al.*, 2020). In brief, leaves of 4-weeks-old plants (Col-0, PsAvh113-L1/L2 lines and *atdpb* mutant) were inoculated with *P. parasitica* PBS042 by adding a droplet containing 2000 zoospores. Approximately 30 inoculated leaves were incubated in plastic plates padded with wet filter paper in a greenhouse at 25 °C for 2 days. Subsequently, disease development was evaluated by measuring and photographing the lesion diameter. In tobacco, expressing *GmDPB*, *GmCAT1* and *PsAvh113* were individually expressed in *N. benthamiana* leaves and followed by *P. parasitica* PBS042 inoculation. In soybean, target genes were transiently transformed in soybean hairy roots mediated by *A. rhizogenes*. Subsequently, hairy roots expressing target gene were inoculated with *P. sojae* RFP-P6497. The number of oospores was counted and the relative biomass of *P. sojae* was assayed. These experiments were repeated three times with similar results.

Microscopy

To detect protein interactions *in vivo*, the full-length coding sequences of the *GmDPB* and *PsAvh113* genes were individually cloned into the YC and YN vectors as previously described (Lu *et al.*, 2010). Combinations of the plasmid constructs (YN-*PsAvh113/PsAvh113*$^{\triangle IR1}$/*PsAvh113*$^{\triangle IR2}$ + YC-*GmDPB*, YN-EV + YC-*GmDPB*, YN-*PsAvh113/PsAvh113*$^{\triangle IR1}$/*PsAvh113*$^{\triangle IR2}$ + YC-EV) were coinfitrated into *N. benthamiana*, respectively. To analyse GmDPB nuclear reposition regulated by PsAvh113 in the epidermal leaves of *N. benthamiana*, *p35S:GmDPB-YFP-HA* or *p35S:PsAvh113/PsAvh113*$^{\triangle IR1}$/*PsAvh113*$^{\triangle IR2}$-CFP constructs were transformed into *Agrobacterium* strain GV3101, respectively. The OD600 of *A. tumefaciens* was brought to an optical density of 1.2, and equal volumes of each culture were mixed for infiltrating the epidermal *N. benthamiana* leaves. YFP fluorescence was excited with the 514-nm line ray of the argon laser and detected in the range between 520 and 540 nm. CFP fluorescence was excited with the 458 nm ray line of the argon laser and recorded in one of the confocal channels in the 465–520 nm emission range. The CFP/YFP signals were imaged 2–3 days after infiltration using an Olympus Fluoview FV3000 confocal laser microscope (Olympus, Tokyo, Japan).

Potato virus X (PVX) infection assays and northern blotting

PCR products of *PsAvh113*, *PsAvh113*$^{\triangle IR1}$ and *PsAvh113*$^{\triangle IR2}$ (without signal peptides) were ligated into pGR106 vector containing the entire PVX genome (Shi *et al.*, 2020). About 2-weeks-old *N. benthamiana* plants were infiltrated with the *A. tumefaciens* (OD = 0.6) harbouring the plasmids pGR106-EV, pGR106-*PsAvh113* and pGR106-*PsAvh113*-muants. After 2–3 weeks, the infiltrated plants were photographed and total RNA of those plants were extracted using Trizol Reagent. Viral RNAs were detected by probes corresponding to the PVX coat protein-encoding gene (CP) as previously described (Qiao *et al.*, 2013; Shi *et al.*, 2020). The accumulation of viral RNAs were quantified based on the new sgRNA expression that produced by PsAvh113 and its mutants. Briefly, 6 μg total RNA were loaded into 1.5% agarose gels containing 10% formaldehyde and 1 × MOPS buffer and run at 100 V for 45 min. Following transfer to a nylon membrane, hybridization with a BIOTIN-labelled probe was performed to detect the 3-prime regions of PVX genome segments.

Nuclear-cytoplasmic fractionation assay

The separation of the nuclear and cytoplasmic fractions was carried out as previously described (Qi *et al.*, 2019). About 0.5 g of the infiltrated leaf tissue was ground in liquid nitrogen and homogenized in 2 mL of lysis buffer (20 mM Tris–HCl, pH 7.5, 20 mM KCl, 2 mM EDTA, 2.5 mM MgCl2, 25% glycerol, 250 mM sucrose, 5 mM DTT and one protease inhibitor cocktail tablet (Roche) per 50 mL) for 10 min at 4 °C. The homogenate was filtered through the Miracloth and then centrifuged at 1500 *g* for 10 min at 4 °C. The centrifuged supernatant was centrifuged at 10 000 *g* for 10 min at 4 °C and the final supernatant was collected as the cytoplasmic fraction. The centrifuged pellet was washed four times with 5 mL of nuclear resuspension buffer (NRBT buffer, 20 mM Tris–HCl, pH 7.4, 25% glycerol, 2.5 mM MgCl2 and 0.2% Triton X-100) at 4 °C, and then the pellet was resuspended with 500 μL of NRB2 (20 mM Tris–HCl, pH 7.5, 0.25 M sucrose, 10 mM MgCl$_2$, 0.5% Triton X-100, 5 mM β-mercaptoethanol and one protease inhibitor cocktail tablet (Roche) per 50 mL). The suspension was laid carefully over 500 μL NRB3 (20 mM Tris–HCl, pH 7.5, 1.7 M sucrose, 10 mM MgCl$_2$, 0.5% Triton X-100, 5 mM β-mercaptoethanol and one protease inhibitor cocktail tablet (Roche) per 50 mL), and then centrifuged at 16 000 *g* for 45 min at 4 °C. Finally, the pellet as the nuclear fraction was resuspended in 400 μL of lysis buffer. As quality controls for the fractionation, Actin/Rubisco (Abmart) and Histone H3 (Abmart) were used as the cytoplasmic and nuclear markers, respectively.

Immunoblot analysis of protein abundance

Protein was extracted from *N. benthamiana* leaves expressing *YFP-GmDPB-MYC*, *YFP-PsAvh113-FLAG* or other *YFP-FLAG* using PEB buffer (25 mM Tris–HCl pH 7.6, 15 mM MgCl$_2$, 150 mM NaCl, 60 mM β-glycerophosphate, 0.1 mM Na$_3$VO$_4$, 1 mM NaF, 1 mM phenylmethanesulfonyl fluoride, 1% Triton X-100). Bradford solution was used to quantify protein concentration. GmDPB and the various concentrations of PsAvh113 or YFP protein were co-incubated at 25 °C for 30 min. The reaction products were detected by SDS-polyacrylamide gel electrophoresis (PAGE) using anti-FLAG (MBL, 1 : 5000 dilution) and anti-MYC (MBL, 1 : 5000 dilution).

Co-immunoprecipitation and western blotting

Co-immunoprecipitation was assayed as described previously (Zhang *et al.*, 2019). In brief, the infiltrated leaves of *N. benthamiana* were harvested at 2 dpi. Then these leaves were powdered equally and mixed in extraction buffer at 4 °C, the suspension was centrifuged and filtered to collect the supernatant. Myc-beads were added to the supernatant and the mixtures were incubated at 4 °C for 1 h. After washing three times, the protein-enriched beads were subjected to western blotting. Proteins were separated in 12% SDS-PAGE gels by electrophoresis, then transferred onto PVDF membrane by semidry electroblotting. The membrane was blocked with TBST (0.01M Tris–HCl, 0.1 M NaCl and 1/1000 Tween 20)-milk solution and incubated with primary mouse anti-Myc (MBL, 1 : 5000 dilution), rabbit anti-HA (MBL, 1 : 1000 dilution) or anti-Flag (MBL, 1 : 5000 dilution) as the primary antibody and anti-mouse/rabbit-HRP (MBL, 1 : 5000 dilution) as the secondary antibody. Signals were developed using Chemiluminescence substrate (Thermo, #34580, USA), then imaged using Amersham Image 600 (GE Healthcare).

Acknowledgements

Conflict of interest statement

The authors declare no competing interests.

Author contributions

YQ conceived and designed the experiments; XGZ, LG, XYZ, RQZ, SH, RZ, DL and JZ performed the experiments. XGZ analysed the experiment data; YQ and XGZ wrote the manuscript. All authors have read and approved the final manuscript.

References

Ai, G., Xia, Q., Song, T., Li, T., Zhu, H., Peng, H., Liu, J. *et al.* (2021) A *Phytophthora sojae* CRN effector mediates phosphorylation and degradation of plant aquaporin proteins to suppress host immune signaling. *PLoS Pathog.* **17**, e1009388.

Chandran, D., Rickert, J., Huang, Y., Steinwand, M.A., Marr, S.K. and Wildermuth, M.C. (2014) Atypical E2F transcriptional repressor DEL1 acts at the intersection of plant growth and immunity by controlling the hormone salicylic acid. *Cell Host Microbe*, **15**, 506–513.

Cheneby, J., Gheorghe, M., Artufel, M., Mathelier, A. and Ballester, B. (2018) ReMap 2018: an updated atlas of regulatory regions from an integrative analysis of DNA-binding ChIP-seq experiments. *Nucleic Acids Res.* **46**, D267–D275.

Cheng, Q., Dong, L., Gao, T., Liu, T., Li, N., Wang, L., Chang, X. *et al.* (2018) The bHLH transcription factor GmPIB1 facilitates resistance to *Phytophthora sojae* in Glycine max. *J. Exp. Bot.* **69**, 2527–2541.

Dat, J.F., Pellinen, R., Beeckman, T., Van De Cotte, B., Langebartels, C., Kangasjarvi, J., Inze, D. *et al.* (2003) Changes in hydrogen peroxide homeostasis trigger an active cell death process in tobacco. *Plant J.* **33**, 621–632.

Datta, A., Sen, J., Hagen, J., Korgaonkar, C.K., Caffrey, M., Quelle, D.E., Hughes, D.E. *et al.* (2005) ARF directly binds DP1: interaction with DP1 coincides with the G1 arrest function of ARF. *Mol. Cell. Biol.* **25**, 8024–8036.

DeGregori, J. and Johnson, D.G. (2006) Distinct and overlapping roles for E2F family members in transcription, proliferation and apoptosis. *Curr. Mol. Med.* **6**, 739–748.

Del Pozo, J.C., Diaz-Trivino, S., Cisneros, N. and Gutierrez, C. (2007) The E2FC-DPB transcription factor controls cell division, Endoreplication and lateral root formation in a SCF-dependent manner. *Plant Signal. Behav.* **2**, 273–274.

Dimova, D.K. and Dyson, N.J. (2005) The E2F transcriptional network: old acquaintances with new faces. *Oncogene*, **24**, 2810–2826.

Girling, R., Partridge, J.F., Bandara, L.R., Burden, N., Totty, N.F., Hsuan, J.J. and La Thangue, N.B. (1993) A new component of the transcription factor DRTF1/E2F. *Nature*, **365**, 468.

Gui, X., Zhang, P., Wang, D., Ding, Z., Wu, X., Shi, J., Shen, Q.H. *et al.* (2022) Phytophthora effector PSR1 hijacks the host pre-mRNA splicing machinery to modulate small RNA biogenesis and plant immunity. *Plant Cell*, **34**, 3443–3459.

Helin, K., Wu, C., Fattaey, A., Lees, J., Dynlacht, B., Ngwu, C. and Harlow, E. (1993) Heterodimerization of the transcription factors E2F-1 and DP-1 leads to cooperative trans-activation. *Genes Dev.* **7**, 1850–1861.

Higo, K., Ugawa, Y., Iwamoto, M. and Korenaga, T. (1999) Plant cis-acting regulatory DNA elements (PLACE) database: 1999. *Nucleic Acids Res.* **27**, 297–300.

Hou, Y., Zhai, Y., Feng, L., Karimi, H.Z., Rutter, B.D., Zeng, L., Choi, D.S. *et al.* (2019) A phytophthora effector suppresses trans-kingdom RNAi to promote disease susceptibility. *Cell Host Microbe*, **25**, 153–165.e155.

Iglesias-Ara, A., Osinalde, N. and Zubiaga, A.M. (2018) Detection of E2F-induced transcriptional activity using a dual luciferase reporter assay. *Methods Mol. Biol.* **1726**, 153–166.

Inaba, J., Kim, B.M., Shimura, H. and Masuta, C. (2011) Virus-induced necrosis is a consequence of direct protein-protein interaction between a viral RNA-silencing suppressor and a host catalase. *Plant Physiol.* **156**, 2026–2036.

Jiao, Z., Tian, Y., Cao, Y., Wang, J., Zhan, B., Zhao, Z., Sun, B. *et al.* (2021) A novel pathogenicity determinant hijacks maize catalase 1 to enhance viral multiplication and infection. *New Phytol.* **230**, 1126–1141.

Jing, M., Guo, B., Li, H., Yang, B., Wang, H., Kong, G., Zhao, Y. *et al.* (2016) A *Phytophthora sojae* effector suppresses endoplasmic reticulum stress-mediated immunity by stabilizing plant binding immunoglobulin proteins. *Nat. Commun.* **7**, 11685.

Jones, J.D. and Dangl, J.L. (2006) The plant immune system. *Nature*, **444**, 323–329.

Jorda, J. and Kajava, A.V. (2010) Protein homorepeats sequences, structures, evolution, and functions. *Adv. Protein Chem. Struct. Biol.* **79**, 59–88.

Kamoun, S., Furzer, O., Jones, J.D., Judelson, H.S., Ali, G.S., Dalio, R.J., Roy, S.G. *et al.* (2015) The Top 10 oomycete pathogens in molecular plant pathology. *Mol. Plant Pathol.* **16**, 413–434.

Kent, L.N. and Leone, G. (2019) The broken cycle: E2F dysfunction in cancer. *Nat. Rev. Cancer*, **19**, 326–338.

Kong, L., Qiu, X., Kang, J., Wang, Y., Chen, H., Huang, J., Qiu, M. *et al.* (2017) A Phytophthora effector manipulates host histone acetylation and reprograms defense gene expression to promote infection. *Curr. Biol.* **27**, 981–991.

Kosugi, S. and Ohashi, Y. (2002a) E2F sites that can interact with E2F proteins cloned from rice are required for meristematic tissue-specific expression of rice and tobacco proliferating cell nuclear antigen promoters. *Plant J.* **29**, 45–59.

Kosugi, S. and Ohashi, Y. (2002b) E2Ls, E2F-like repressors of Arabidopsis that bind to E2F sites in a monomeric form. *J. Biol. Chem.* **277**, 16553–16558.

Kovesdi, I., Reichel, R. and Nevins, J. (1987) Role of an adenovirus E2 promoter binding factor in E1A-mediated coordinate gene control. *Proc. Natl. Acad. Sci. USA*, **84**, 2180–2184.

Lammens, T., Li, J., Leone, G. and De Veylder, L. (2009) Atypical E2Fs: new players in the E2F transcription factor family. *Trends Cell Biol.* **19**, 111–118.

Levdansky, E., Romano, J., Shadchan, Y., Sharon, H., Verstrepen, K.J., Fink, G.R. and Osherov, N. (2007) Coding tandem repeats generate diversity in *Aspergillus fumigatus* genes. *Eukaryot. Cell*, **6**, 1380–1391.

Lin, Y., Hu, Q., Zhou, J., Yin, W., Yao, D., Shao, Y., Zhao, Y. *et al.* (2021) *Phytophthora sojae* effector Avr1d functions as an E2 competitor and inhibits ubiquitination activity of GmPUB13 to facilitate infection. *Proc. Natl. Acad. Sci. USA*, **118**, e2018312118.

Liu, T., Ye, W., Ru, Y., Yang, X., Gu, B., Tao, K., Lu, S. *et al.* (2011) Two host cytoplasmic effectors are required for pathogenesis of *Phytophthora sojae* by suppression of host defenses. *Plant Physiol.* **155**, 490–501.

Liu, H., Su, J., Zhu, Y., Yao, G., Allan, A.C., Ampomah-Dwamena, C., Shu, Q. *et al.* (2019) The involvement of PybZIPa in light-induced anthocyanin accumulation via the activation of PyUFGT through binding to tandem G-boxes in its promoter. *Hortic. Res.* **6**, 134.

Lu, Q., Tang, X., Tian, G., Wang, F., Liu, K., Nguyen, V., Kohalmi, S.E. *et al.* (2010) Arabidopsis homolog of the yeast TREX-2 mRNA export complex: components and anchoring nucleoporin. *Plant J.* **61**, 259–270.

Lu, X., Yang, Z., Song, W., Miao, J., Zhao, H., Ji, P., Li, T. *et al.* (2023) The *Phytophthora sojae* effector PsFYVE1 modulates immunity-related gene expression by targeting host RZ-1A protein. *Plant Physiol.* **191**, 925–945.

Ma, L.S., Wang, L., Trippel, C., Mendoza-Mendoza, A., Ullmann, S., Moretti, M., Carsten, A. *et al.* (2018) The Ustilago maydis repetitive effector Rsp3 blocks the antifungal activity of mannose-binding maize proteins. *Nat. Commun.* **9**, 1711.

Mao, C., He, J., Liu, L., Deng, Q., Yao, X., Liu, C., Qiao, Y. *et al.* (2020) OsNAC2 integrates auxin and cytokinin pathways to modulate rice root development. *Plant Biotechnol. J.* **18**, 429–442.

Mariconti, L., Pellegrini, B., Cantoni, R., Stevens, R., Bergounioux, C., Cella, R. and Albani, D. (2002) The E2F family of transcription factors from Arabidopsis thaliana. Novel and conserved components of the retinoblastoma/E2F pathway in plants. *J. Biol. Chem.* **277**, 9911–9919.

Mathioudakis, M.M., Veiga, R.S., Canto, T., Medina, V., Mossialos, D., Makris, A.M. and Livieratos, I. (2013) Pepino mosaic virus triple gene block protein 1 (TGBp1) interacts with and increases tomato catalase 1 activity to enhance virus accumulation. *Mol. Plant Pathol.* **14**, 589–601.

Mhamdi, A., Queval, G., Chaouch, S., Vanderauwera, S., Van Breusegem, F. and Noctor, G. (2010) Catalase function in plants: a focus on Arabidopsis mutants as stress-mimic models. *J. Exp. Bot.* **61**, 4197–4220.

Mueller, O., Kahmann, R., Aguilar, G., Trejo-Aguilar, B., Wu, A. and de Vries, R.P. (2008) The secretome of the maize pathogen Ustilago maydis. *Fungal Genet. Biol.* **45**(Suppl 1), S63–S70.

Mur, L.A., Kenton, P., Atzorn, R., Miersch, O. and Wasternack, C. (2006) The outcomes of concentration-specific interactions between salicylate and jasmonate signaling include synergy, antagonism, and oxidative stress leading to cell death. *Plant Physiol.* **140**, 249–262.

O'Dushlaine, C.T., Edwards, R.J., Park, S.D. and Shields, D.C. (2005) Tandem repeat copy-number variation in protein-coding regions of human genes. *Genome Biol.* **6**, R69.

Perrot-Rechenmann, C. (2010) Cellular responses to auxin: division versus expansion. *Cold Spring Harb. Perspect. Biol.* **2**, a001446.

Petrov, V.D. and Van Breusegem, F. (2012) Hydrogen peroxide—a central hub for information flow in plant cells. *AoB PLANTS*, **2012**:pls014.

Qi, T., Guo, J., Liu, P., He, F., Wan, C., Islam, M.A., Tyler, B.M. *et al.* (2019) Stripe rust effector PstGSRE1 disrupts nuclear localization of ROS-promoting transcription factor TaLOL2 to defeat ROS-induced defense in wheat. *Mol. Plant*, **12**, 1624–1638.

Qiao, Y., Liu, L., Xiong, Q., Flores, C., Wong, J., Shi, J., Wang, X. *et al.* (2013) Oomycete pathogens encode RNA silencing suppressors. *Nat. Genet.* **45**, 330–333.

Roshan, P., Kulshreshtha, A., Kumar, S., Purohit, R. and Hallan, V. (2018) AV2 protein of tomato leaf curl Palampur virus promotes systemic necrosis in *Nicotiana benthamiana* and interacts with host Catalase2. *Sci. Rep.* **8**, 1273.

Rudd, J.J., Antoniw, J., Marshall, R., Motteram, J., Fraaije, B. and Hammond-Kosack, K. (2010) Identification and characterisation of *Mycosphaerella graminicola* secreted or surface-associated proteins with variable intragenic coding repeats. *Fungal Genet. Biol.* **47**, 19–32.

Shi, J., Zhu, Y., Li, M., Ma, Y., Liu, H., Zhang, P., Fang, D. *et al.* (2020) Establishment of a novel virus-induced virulence effector assay for the identification of virulence effectors of plant pathogens using a PVX-based expression vector. *Mol. Plant Pathol.* **21**, 1654–1661.

Song, T., Ma, Z., Shen, D., Li, Q., Li, W., Su, L., Ye, T. *et al.* (2015) An oomycete CRN effector reprograms expression of plant HSP genes by targeting their promoters. *PLoS Pathog.* **11**, e1005348.

Tyler, B.M., Tripathy, S., Zhang, X., Dehal, P., Jiang, R.H., Aerts, A., Arredondo, F.D. *et al.* (2006) Phytophthora genome sequences uncover evolutionary origins and mechanisms of pathogenesis. *Science*, **313**, 1261–1266.

Vlieghe, K., Boudolf, V., Beemster, G.T., Maes, S., Magyar, Z., Atanassova, A., de Almeida Engler, J. *et al.* (2005) The DP-E2F-like gene DEL1 controls the endocycle in *Arabidopsis thaliana*. *Curr. Biol.* **15**, 59–63.

Wang, Y. and Wang, Y. (2018) *Phytophthora sojae* effectors orchestrate warfare with host immunity. *Curr. Opin. Microbiol.* **46**, 7–13.

Wang, S., Gu, Y., Zebell, S.G., Anderson, L.K., Wang, W., Mohan, R. and Dong, X. (2014) A noncanonical role for the CKI-RB-E2F cell-cycle signaling pathway in plant effector-triggered immunity. *Cell Host Microbe*, **16**, 787–794.

Wang, Y., Tyler, B.M. and Wang, Y. (2019) Defense and counterdefense during plant-pathogenic oomycete infection. *Annu. Rev. Microbiol.* **73**, 667–696.

Yang, T., Qiu, L., Huang, W., Xu, Q., Zou, J., Peng, Q., Lin, H. *et al.* (2020) Chilli veinal mottle virus HCPro interacts with catalase to facilitate virus infection in *Nicotiana tabacum*. *J. Exp. Bot.* **71**, 5656–5668.

Yuan, H.M., Liu, W.C. and Lu, Y.T. (2017) CATALASE2 coordinates SA-mediated repression of both auxin accumulation and JA biosynthesis in plant defenses. *Cell Host Microbe*, **21**, 143–155.

Zhang, M., Li, Q., Liu, T., Liu, L., Shen, D., Zhu, Y., Liu, P. *et al.* (2015) Two cytoplasmic effectors of *Phytophthora sojae* regulate plant cell death via interactions with plant catalases. *Plant Physiol.* **167**, 164–175.

Zhang, P., Jia, Y., Shi, J., Chen, C., Ye, W., Wang, Y., Ma, W. *et al.* (2019) The WY domain in the Phytophthora effector PSR1 is required for infection and RNA silencing suppression activity. *New Phytol.* **223**, 839–852.

Zhu, X., He, S., Fang, D., Guo, L., Zhou, X., Guo, Y., Gao, L. *et al.* (2020) High-throughput sequencing-based identification of Arabidopsis miRNAs induced by *Phytophthora capsici* infection. *Front. Microbiol.* **11**:1094.

Supporting information

Additional supporting information may be found online in the Supporting Information section at the end of the article.

Figure S1 PVX-based recombinant construct and expression pattern of *PsAvh113*.

Figure S2 Overexpression of *PsAvh113* affects plant development and defence response in *Arabidopsis*.

Figure S3 Analysis of PsAvh113 and its mutated derivatives by subcellular localization, the cytoplasm and the nucleus protein separation.

Figure S4 The nuclear localization of PsAvh113 is required for its virulence activity in plants.

Figure S5 Analysis of interaction between PsAvh113 and GmDPB *in vitro* and *in vivo*.

Figure S6 DPB genes in soybean and *Arabidopsis* positively regulate plant immunity against *Phytophthora* infection.

Figure S7 PsAvh113 affects the stability of GmDPB protein in cytoplasm and nucleus.

Figure S8 Analysis of subcellular localization and expression of *GmCAT1*.

Figure S9 Analysis of expression and editing sequence in *GmCAT1*-overexpressed and *pGmCAT1 or GmCAT1*-edited soybean hairy roots.

Table S1 Primers used in this study.